Global geodetic signatures of the Antarctic ice sheet

Thomas S. James

Geological Survey of Canada, Sidney, British Columbia

Erik R. Ivins

Jet Propulsion Laboratory, California Institute of Technology, Pasadena

Abstract. Four scenarios of present day Antarctic ice sheet mass change are developed from comprehensive reviews of the available glaciological and oceanographic evidence. The gridded scenarios predict widely varying contributions to secular sea level change $\dot{\xi}$ ranging from -1.1 to 0.45 mm/yr, and predict polar motion $\dot{\mathbf{m}}$ and time-varying low-degree gravitational coefficients J_l that differ significantly from earlier estimates. A reasonably linear relationship between the rate of sea level change from Antarctica $\dot{\xi}_A$ and the predicted Antarctic J_l is found for the four scenarios. This linearity permits a series of forward models to be constructed that incorporate the effects of ice mass changes in Antarctica, Greenland, and distributed smaller glaciers, as well as postglacial rebound (assuming the ICE-3G deglaciation history), with the goal of obtaining optimum reconciliation between observed constraints on J_l and sea level rise $\dot{\xi}$. Numerous viable combinations of lower mantle viscosity and hydrologic sources are found that satisfy "observed" $\dot{\xi}$ in the range of 1 to 2-2.5 mm/yr and observed J_l for degrees 2, 3, and 4. In contrast, rates of global sea level rise above 2.5 mm/yr are inconsistent with available J_l observations. The successful composite models feature a pair of lower mantle viscosity solutions, arising from the sensitivity of J_l to glacial rebound. The paired values are well separated at $\dot{\xi}$ = 1 mm/yr, but move closer together as $\dot{\xi}$ is increased, and, in fact, merge around $\dot{\xi}$ = 2 - 2.5 mm/yr, revealing an intimate relation between $\dot{\xi}$ and preferred lower mantle viscosity. This general pattern is quite robust and persists for different J_l solutions, for variations in source assumptions, and for different styles of lower mantle viscosity stratification. Tighter J_l constraints for $l > 2$ may allow some viscosity stratification schemes and source assumptions to be excluded in the future. For a given total observed $\dot{\xi}$, the sea level rise from Antarctica $\dot{\xi}_A$ is tightly constrained and ranges from 0 to +1 mm/yr (corresponding to an ablating ice sheet) as estimates of $\dot{\xi}$ are raised from 1 to 2.5 mm/yr. However, when the degree 3 zonal harmonic constraint is removed, the solutions show little sensitivity to Antarctic mass balance, emphasizing the need for a well determined odd-degree secular zonal harmonic for determining polar ice mass balance.

Introduction

It has long been known that ocean-continent hydrological exchanges could produce predictable changes in global geodetic observables such as the length of day, the long wavelength gravitational field.11, and the location of the pole of rotation $\mathbf{m}$ [e.g., *Munk and Revelle*, 1952; *Lambeck and Cazenave*, 1976; *Lambeck*, 1980]. Spurred by the current interest in global change studies and by advances in satellite geodesy, recent work has been undertaken to determine the effects of hydrological exchanges on global geodetic observables [*Wagner and McAdoo*, 1986; *Sabadini et al.*, 1988; *Chao and O'Connor*, 1988a, b; *Mitrovica and Peltier*, 1989, 1993; *Trupin et al.*, *1992; Ivins et al., 1993; Trupin*, 1993; *James and Ivins, 1995].* Several of these studies have considered the effect of present day mass changes of the Antarctic and Greenland ice sheets and mountain glaciers and small ice caps. The delayed viscoelastic response of the Earth to late Pleistocene and early Holocene deglaciations also produces a significant signature [*Yoder et al.*, 1983; *Peltier*, 1983; 1985; *Rubincam, 1984; Yuen and Sabadini*, 1985; *Yuen et al., 1986],* and this is superimposed on the present day climate change related signature.

The volume of icc grounded onto the Antarctic continent is immense, accounting for about 2.1% of tbc total supracrustal water supply. Nonglacial water outside of the world's ocean basins, by contrast, amounts to a mere 0.3°/0. Furthermore, small mountain glaciers (plus icc caps) and icc grounded in Greenland total to only 0.006% and 0.21 %, respectively [*Meier*, 1990]. Estimates of the present day balance state of tbc great Antarctic icc sheet remain contentious, and a small fractional imbalance can translate into a large, perhaps even dominant, influence on the sca level rise budget. What is proposed in this paper is to assume, a priori, that the mass balance state for Antarctica is unknown. An Antarctic mass balance constraint might then be devised by parameterizing alternative sources for sea level and secular, time-dependent gravity and polar motion. This undertaking, is initiated by evaluating a number of scenarios of present day Antarctic mass balance based on accumulation data and drainage basin analyses [*Giovinetto and Bentley*, 1 985; *Bentley and Giovinetto, l991; Bentley, 1 995]* and oceanographic constraints [*Jacobs et al.*, 1992], The scenarios differ mainly in how mass balance is extrapolated to unmeasured regions. A sum of the mass balance of each drainage system yields a prediction of the net hydrological balance of the entire grounded Antarctic ice sheet M and hence Antarctica's contribution to present day sca level rise $\dot{\xi}_4$.

Wc then proceed to search for combinations of present day sca level sourcing and mantle viscosity input to postglacial rebound that satisfy observed constraints on satellite derived $\dot{J}_l$ and total (global) sca level rise $\dot{\xi}$. The Antarctic contribution to sca level rise $\dot{\xi}_4$ is treated as a free parameter, and we utilize linear relationships between $\dot{\xi}_4$ and low-degree secular zonal harmonics $\dot{J}_l$ derived from tbc scenarios developed here. This procedure also requires treating tbc unknown Greenland contribution, $\dot{\xi}_G$, in a similar manner, and assumes that total sca level rise is bracketed by the range 1 to 2.5 mm/yr [*Douglas*, 1995]. Although no attempt is made to solve a formal leas! squares inversion, a parameter search indicates tbc sensitivity of $\dot{\xi}_4$ to $\dot{J}_l$. It appears that optimized sourcing for tbc satellite solutions for secular $\dot{J}_l$ (l = 2- 4) imply an Antarctic icc sheet in a state of negative mass balance. in large measure, the predicted polar motion $\dot{\mathbf{m}}$ plays a secondary role since polar motion is less sensitive to Antarctic mass imbalance than to other, relatively non-zonal mass redistributions such as mountain glacier melting or Greenland imbalance [*Wahr et al.*, 1993]. Lower mantle viscosity is also freed as a parameter in tbc prediction of tbc glacial rebound $\dot{J}_l$ values, and wc find that a broad range of viscosity values can satisfy the data.

However, there arc some important caveats in reaching this conclusion. First, tbc influence of postglacial rebound on $\dot{J}_l$ is sensitive to glacial load history, The late Pleistocene and early Holocene load history must be spatially and temporally well approximated by tbc ICE-3G model [*Tushingham and Peltier, 1991*]. This sensitivity is related to the prediction of a relatively large positive J_3, which would not occur if Antarctic deglaciation were to occur earlier and more "in phase" with tbc northern hemisphere deglaciation [e.g., *Ivins c/ al., 1993],* Second, each of three portions of the sca level rise budget (small mountain glaciers and icc caps, anthropogenic sources, and steric expansion) should be known to witbin a factor of about 2 and generally consistent with tbc reports by *Meier*

[1 990], Warrick and Oerlemans [1 990], Douglas [1 995], *Chao [* 1995], and *de Wolde et al.* [199 S]. I'bird, the Antarctic sea level/L/l parameterizations must not change significantly from those found for our four scenarios.

Most critical to the analysis of the Antarctic balance state is the existence of a robust $\dot{J}_3$ solution from satellite laser ranging data. That a stable solution for $\dot{J}_3$ has yet been obtained is somewhat debatable [*Eanes and Bettadpur*, 1996; *Nerem and Klosko*, 1996; *Cazenave et al.*, 1996]. It has been discovered recently that there is a strong correlation between a known nongravitational force (Earth albedo) and the residuals of the LAGEOS1 eccentricity orbital element [*Martin and Rubincam*, 1996]. Residuals in those particular elements tend to dominate multi satellite solutions for the odd-degree gravity harmonics [*Eanes and Bettadpur*, 1996], and it would not be too surprising to see a series of future revisions of secular $\dot{J}_3$. Therefore our analysis may have a more modest conclusion: an isolation of a strong sensitivity of satellite-determined $\dot{J}_3$ to the present day Antarctic mass balance state.

A state of negative Antarctic mass balance is generally at odds with what glaciologists have concluded from analyses of the major ice drainage systems [*Bentley and Giovinetto, 1991]* unless ice shelf basal melting and calving rates have been substantially underestimated as suggested recently by *Jacobs et al.* [1992]. Ultimately, the confirmation of the globally based solutions for $\dot{\xi}_A$ that rely on $\dot{J}_l$ and $\dot{\mathbf{m}}$ must be found through a more detailed analysis of the mass balance of these drainage basins.

This paper expands on some of the results presented by *James and Ivins [1995]* and is part of a broader study considering all the geodetic responses due to Antarctic ice mass change. Only recently has there been interest in the local geodetic signatures of vertical and horizontal crustal motion and changes in the solid surface gravity that rapidly evolving ice masses might produce [*Conrad and Hager*, 1995; *Jetties and Ivins*, 1995; *Wahr et* al., 1995]. *James and Ivins [1995]* found that one of their scenarios predicted a maximum peak vertical crustal motion rate of ≈ 10 mm/yr, large enough to be detectable using a series of Global Positioning System (GPS) data collected in continuous observing mode. However, glacial rebound might drive stronger vertical crustal motions in West Antarctica if current models (ICE-3G or ICE-4G) of a large-volume, mainly Holocene reduction of the Antarctic ice mass are correct. A more detailed description of the crustal motion calculations are to be presented in a later paper.

The first part of this paper describes in some detail the background and development of four scenarios of present day Antarctic mass change Following that is a discussion of the resulting global geodetic predictions and a comparison with observations and other possible sources. We conclude by describing global composite scenarios that simultaneously satisfy observed constraints on $\dot{J}_l$ and sea level change $\dot{\xi}$. First, we comment further on present day sea level change.

Present Day Sea Level Change and Antarctic Ice Sheet Mass Balance

There is a wide consensus that over the past few decades, sea level has been rising, with recent analyses finding a sea

level rise between 1 and 2.5 mm/yr [*Barnett, 1983; Peltier and Tushingham, 1 989; Trupin and Wahr,* 1 *990; Douglas, 1991; Meier,* 1*993].* However, these values contrast sharply with estimates of total sea level rise that are obtained when the input from known sources is considered. For example, *Meier [1993]* estimated that *0.4 ± 0.2* mm/yr of sea level rise. comes from mountain glaciers and small ice caps, *-0.2 ± 0.4* mm/yr *from* Greenland, *-0,45 ± 0.55* mm/yr from Antarctica, 0.4 ± 0.2 mm/yr from ocean thermal expansion, and 0.23 ± 0.24 mm/yr from land hydrology. These inputs sum to 0.4 ± 0.8 mm/yr (root-sum-square error), significantly below the amount of sea level rise obtained from most analyses of tide gauge records. It is clear that our understanding of the various factors contributing to sea level change is incomplete.

Estimates of the net mass balance of Antarctica vary widely due 10 uncertainties in determining both accumulation and discharge rates. The mass accumulation rate in Antarctica is around 2×10^{15} kg/yr *(2000* Gt/yr); a 10°/0 net imbalance is sufficient to cause sea level to change by about *0.6* mm/yr (adding 360 Gt of water to the oceans causes sea level to rise by about 1 mm). The Intergovernmental I'anl on Climate Change (1['('(') estimates of the contribution to sea level change in the past 100 years from Antarctica range from -0. S to 0,5 mm/yr [*Warrick and Oerlemans,* 1990], indicating that a mass imbalance of either sign and equivalent to ≈10% of the accumulation rate is plausible. A recent update to the IPCC report [*Warrick et* 01,, 1996] *gives* an even broader range of ±1.4 mm/yr. In the following section we discuss scenarios extracted from two detailed studies of Antarctic mass balance, A study by *Bentley and Giovinetto* [1 99 1] found the Antarctic contribution to sea level rise to be negative ($-0.1 \geq \dot{\xi}_A \geq -1.1$ mm/yr), and another by *Jacobs et al.* [1992] found that the Antarctic contribution to sea level rise $\dot{\xi}_A$ could be as large as + 1.3 mm/yr

Drainage Basin Analysis

To obtain a regional net mass balance, it is necessary to evaluate both mass input and output of the ice sheet. The maw input of a region, assuming that there is no inflow from surrounding areas, comes from surface accumulation, Net surface accumulation is due to a number of processes, to which precipitation and drifting contribute positively, and sublimation and deflation (wind erosion) contribute negatively. *Bentley and Giovinetto [1 991]* (hereinafter referred to as BG91) utilized the net surface mass balance estimates of *Giovinetto and Bentley* [1985], a compilation and synthesis of surface mass balance measurements reported in the literature, which BG91 updated to incorporate new data.

Figure 1 illustrates the six major Antarctic drainage systems, as described by *Giovinetto and Bentley [* 1985] and utilized by BG91 **in** their analysis of present day Antarctic ice mass balance. The boundaries of the drainage systems were chosen by determining the regions which feed the three major ice shelves (Amery Ice Shelf, system BoC; Ross Ice Shelf, system EoF; and Filchner-Ronne Ice Shelf, system JoK). These three systems drain much of the interior of Antarctica, The remaining three systems (Ka'B, CcE, and Fj'J) tend to drain coastal regions. The drainage systems were then subdivided to obtain physiographically simpler regions [*Giovinetto and Bentley,*

1985]. The boundaries of the subsystems were chosen to follow flow lines, continental divides, or divides separating regions of convergent or divergent flow, thus ensuring that there is little or no mass flow across boundaries.

Ice flow in Antarctica terminates in tbc ocean, As ice flows from the interior, its thickness diminishes, reaching a point where it floats, if the bed is far enough below sca level. The boundary between icc which is supported by the solid surface and floating icc is known as tbc grounding line (Figure *2).* For determining tbc contribution to sca level change, it is the net mass balance of the grounded portions of tbc icc sheet that is important since floating portions arc part of the ocean system. Ideally, then, observations of the rate of outflow of the icc sheet at the grounding line, combined with observations of tbc surface mass balance of the interior portions, would suffice to determine the net mass imbalance of a drainage system. Unfortunately, in dynamically active regions such as ice streams, icc flow can be quite complex and temporally varying [*Bindschadler et al., 1993].*

in practice, observations may only be available inland of the grounding line or close to tbc icc shelf front. If observations are made on the icc shelf (and observations at the grounding line arc kicking,), then it is also necessary to consider the rate at which the shelf is gaining or losing mass owing to basal melting or freezing. Advances in space-based and airborne precise mapping methods will offer a powerful new database in the future. } lowever, these techniques have been in use for an insufficient amount of time 10 yield unambiguous estimates of mass change over most of the great icc sheets [*Fahnestock et al.*, 1993; *Krabill et al.*, 1 995].

Il(i91 began by considering mass imbalance measurements for inland regions (Table 1 and Figure 3). '1'able 1 shows both their regional mass imbalance estimates and their subjective estimate of its significance, essentially defined by measurement accuracy and completeness in coverage. Also shown in 'fable 1 arc the areas and equivalent icc height change rates inferred for the present study. These arc to be described in more detail in the following section. I'able 1 shows that only three inland systems, Lambert Glacier, East Antarctica onto Ross Ice Shelf, and Pine island Glacier, arc considered to have a significant imbalance. Of these, tbc Lambert Glacier bas two conflicting: estimates of accumulation [*Allison, 1979; Allison e/ al.*, 1985; *McIntyre*, 1985a, b], leading to two differing estimates of the net imbalance, onc of which BG91 considered to be significant. A recent reanalysis of the mass balance of the Pine island Glacier system [*Lucchita et al.*, 1995] shows it may be less positive than stated by BG91, although uncertainties still exist.

BG91 next considered icc shelf systems for which there are measurements. 'I 'hey evaluated inflow and outflow of the East and West Ross Icc Shelf and the Amery Icc Shelf and determined the amount of icc shelf basal melting (freezing) required for steady state balance. They did not find evidence to suggest that these regions arc significantly out of balance.

Finally, BG91 considered combined inland and ice shelf systems (1'able 2 and Figure 4). These systems lack outflow measurements al the grounding line and hence require an estimate of the icc shelf basal melting rate required for steady state. Table 2 shows the net mass imbalance, tbc basal melt rate which would be required for steady state, and their

assessment of whether this rate is reasonable. The Amery ICC Shelf and Eastern Ronne Icc Shelf require unreasonably large basal melting rates and the Brunt-1 Riiser-Larsen Ice Shelves require smaller melt rates than those observed. It is suggested, therefore, that these systems have a net mass imbalance.

Scenario Development

BG91 extrapolated the observed net mass imbalances to unmeasured regions in a number of ways, producing balance scenarios for the entire Antarctic ice sheet with the predicted contribution to sca level rise $\dot{\xi}_A$ ranging from -0.1 to -1.1 mm/yr. One of the striking, aspects of mass balance studies in Antarctica are the large regions (approximately 30% by area) for which there arc insufficient observations (Figure 5). The unmeasured regions tend to be coastal regions where mass accumulation rates arc high.

In this study wc have gridded Antarctica with 280 disks of area S0,000 km^2, and for each scenario wc have assigned a net mass balance to each disk (in millimeters pcr year of ice equivalent). This grid is sufficiently fine that ail the regions listed in Tables 1 and 2 can be represented. The final two columns of Table 1 show the areas obtained from gridding the measured regions and , the calculated equivalent icc height change $\dot{\eta}$, where $\dot{\eta} = \dot{M}/(\text{Area} \times \rho_{ice})$ with the density of ice $\rho_{ice} = 917.4$ kg/m^3.

In BG91's minimum scenario they assumed that the ice sheet is in balance except for measured regions which are significantly out of balance (scenario 1, Figure 6a). The McIntyre interpretation for the Lambert Glacier is assumed (1'able 1), and it is assumed that the imbalance of the Amery Icc Shelf is due entirely to processes on the ice shelf ('1'able 2). Furthermore, it is assumed that the entire Filchner-Ronne system is in balance. This leaves the following three regions with a significant imbalance: a growing Pine island glacier ($\dot{M}$ = s() Gt/yr, $\dot{\eta}$ = 218 mm/yr), a growing East Antarctica onto tbc Ross Ice Shelf ($\dot{M}$ = 26 Gt/yr, $\dot{\eta}$ = 16 mm/yr), and a reducing region located inland of the Brunt and Riiser-Larsen Ice Shelves ($\dot{M}$ = -37 Gt/yr, $\dot{\eta}$ = -201 mm/yr). This scenario gives a iow prediction for Antarctica's possible negative contribut ion to sea, level rise ($\dot{\xi}_A$. -0.1 mm/yr) and positive net mass imbalance (A4 = 39 Gt/yr).

tl~91 next extrapolated from measured inland drainage systems to unmeasured regions in two different ways, finding net mass imbalances $\dot{M}$ of 400 and 290 Gt/yr, corresponding to sea level fall of I. 1 and 0.8 mm/yr, respectively. First, they extrapolated to unmeasured regions by assuming that mass imbalancc is proportional to mass input (scenario 2 by mass, Figure 6b). '1'able 1 shows the total net mass imbalance of the measured inland systems to be + 118. S Gt/yr. BG91 found that the mass input to Antarctica is 1660 Gt/yr, and that to the measured systems is 500 Gt/yr. If tbc net mass imbalance of the unmeasured regions is proportional to mass input, then this implies a net mass imbalance of unmeasured regions of 118.5 Gt/yr x (1660 - 500)/500 ≈ + 280 Gt/yr. In gridding scenario 2 by mass, wc concentrated the extrapolated imbalance in coastal disks, where accumulation rates arc highest, For 48 coastal disks, with total area of 2.4 x 10^6 km^2, we determined the equivalent icc height change $\dot{\eta}$ to be 128 mm/yr, giving a total net mass balance $\dot{M}$ of 400 (≈ 280 + 118.5) Gt/yr. Scenario 2

by mass provides a sea level fall of 1.1 mm/yr ($\dot{M}$ = + 400 Gt/yr), the largest of all the scenarios,

lKi91 also extrapolated from measured grounded regions to unmeasured regions by area (scenario *2* by area, Figure 6c). Table 1 shows that our total gridded area of the measured inland regions is 5.3 x 10^6 km^2, which closely approximates BG91's determination of S. 1 x 10^6 km^2. BG91 determined the total grounded area to be 12.1 x 10^6 km^2. This leads to a net mass imbalance of unmeasured regions of + 118.5 Gt/yr x (12.1 - S,1)/5.1 = +163 Gt/yr. For 151 disks in unmeasured areas we determined an equivalent ice height change $\dot{\eta}$ = 24.8 ≈ 25 mm/yr. This corresponds to a net mass imbalance in unmeasured regions of + 172 Gt/yr, chosen to obtain a total net mass balance of +290 (= 172 + 11 8.5) Gt/yr, which is in agreement with the total balance given by BG91. This scenario gives a sea level fall of 0.8 mm/yr ($\dot{M}$ = + 29(1 Gt/yr). Note that because scenarios 2 by mass and by area are extrapolations from inland regions, they lack the mass imbalance near the Brunt and Riiser-Larsen Ice Shelves ($\dot{\eta}$ = - 201 mm/yr) that is present in scenario 1.

1{(;91 presented two additional scenarios, where they extrapolated from all measured areas, not just grounded ice. These scenarios give intermediate values of sea level fall (0.3 and 0.4 mm/yr), and have not been explicitly considered in this study.

A Reappraisal of oceanographic Constraints

The three preceding scenarios predict sea level fall due to Antarctica's net hydrological imbalance at levels ranging from 0.1 to 1.1 mm/yr. If correct, this imbalance contributes to an even larger shortfall between the observed secular sea level rise and the sum of the individual source estimates. One possible resolution of this shortfall is offered in the analysis of *Jacobs et al.* [1992] (hereinafter referred to as J92), who found a negative net mass imbalance for Antarctica. J92 evaluated the net mass balance of both the grounded and floating portions of the Antarctic ice sheet. This is in contrast to BG91, who focused on finding the net mass balance of the grounded portion only. Because J92 considered the ice sheet in toto, they skirted the difficult issue of determining downstream ice fluxes in the grounded regime. Using the estimates of *Giovinetto and Bentley* [1985], with some adjustments in the Antarctic Peninsula, J92 obtained a net mass input for the entire ice sheet of 2144 Gt/yr. They then determined the attrition rates from iceberg calving (-2016 Gt/yr), ice shelf melting (-544 Gt/yr) and runoff (-53 Gt/yr), for a net mass imbalance of the entire ice sheet of -469 Gt/yr. "1 he associated uncertainty is large (±639 Gt/yr). '1 his indicates that one end-member interpretation allows a near zero or slightly positive net mass imbalance for Antarctica, On the other hand, if shelf dissipation rates are in equilibrium with the mass flux out of grounded regions along, the coastline of the Weddell Sea, then the grounded Antarctic ice sheet may have a net hydrological imbalance of -469 Gt/yr, implying an Antarctic contribution to sea level change $\dot{\xi}_4$ = 1.3 mm/yr.

in J92's analysis, ice shelf melting assumes greater significance than in most previous studies. Estimates of ice shelf melting from five previous studies (see J92, I'able 2) average to -322 Gt/yr. J92's estimate, at -S44 Gt/yr, is larger by -222 Gt/yr. This difference accounts for nearly one-half of the total ice sheet mass balance estimate of -469 Gt/yr. 'I'heir

analysis of ice shelf melting, involved consideration of direct measurements of ice shelf thinning and thickening, as well as observations of seawater oxygen isotope ratios, ocean salinity, and thermal structure, and is supported by Ocean Circulation modeling. Salinity variations arc indirect indicators of icc melt rates since salinity is affected by fresh water flushing out of a dissipating icc shelf [*Jenkins and Doake, 199* I; *Hellmer and Jacobs*, 1992].

A Modified Scenario to Account for Observations of Subshelf Meltwater Flow

Constructing a mass balance scenario based on J92's analysis requires apportioning the net mass imbalance between grounded and floating ice because floating ice is already part of the ocean system and dots not contribute further to sea level change. J92 noted that their finding could imply a variety of conditions, ranging from assuming that tbc mass loss is derived entirely from within tbc icc shelves (with grounded icc maintaining its mass) to assuming that the mass loss is due entirely to an enhanced outward flux of grounded icc (with ice shelves maintaining their mass), J92 further noted that Icss than half of the negative net mass imbalance of -469 Gt/yr, equal to $\dot{\xi}_A$ = +1.3 mm/yr, must come from the grounded ice sheet if it were to account for the 0.45 mm/yr shortfall between the 1990 IPCC estimates of the observed total rise rate, $\dot{\xi}$ = 1.S mm/yr [*Warrick and Oerlemans*, 1990], and the sums of known sources and sinks ($\dot{\xi} \approx$ 1.0S mm/yr). The latter are summarized as arising from thermal expansion ($\approx$ 0.4 mm/yr), mountain glaciers ($\approx$ 0.4 mm/yr), Greenland ($\approx$ 0,25 mm/yr) and Antarctica ($\approx$ 0,0 mm/yr).

in constructing a mass balance scenario from J92, wc have made two assumptions. First, the mass imbalance of the interior portions of tile grounded icc is assumed to be adequately described by scenario 2 by area ($\dot{M}$ = 290 Gt/yr). This scenario accounts for net mass balance observations of inland ice where such observations exist, provides a rationale for extrapolating to unmeasured inland regions, and does not have the extreme value of sea level change of scenario 2 by mass, Second, the net mass balance of the grounded portions of the ice sheet is assumed to be sufficient to make up tbc IPCC shortfall of 0.45 mm/yr of sea level rise ($\dot{M}$ = - 160 Gt/yr). These assumptions imply that tbc net mass imbalance of inland portions of tbc grounded Antarctic icc sheet is reasonably well constrained (anti described by scenario 2 by area) but that there is substantial mass loss of grounded ice at or near the grounding line. The mass loss could be due to retreat of tbc grounding line or thinning of the grounded ice sheet near the grounding line. For the grid size adopted in this study, it is not possible to distinguish between the two. Qualitatively, these assumptions seem to be entirely consistent with the studies of *Bentley and Giovinetto [1991]* and *Jacobs et al.* [1992].

'1 herefore 450 Gt/yr (= -160 Gt/yr -290 Gt/yr) was removed from the border of scenario 2 by area to obtain the J92 scenario (Figure 6d). The icc shelf melting rates of J92 were used as an approximate guide to determine where mass should bc removed. '1'able 3 shows the net icc shelf melt rates determined by J92 for four major ice shelf systems and the narrower shelf systems distributed around tbc circumference of Antarctica labeled "within 100 km of ice fronts", Also shown for each ice

shelf system is the net melt rate expressed as a percentage of the total net melt rate. The final columns of I'able 3 show the mass removed from the areas just inland of the various shelf systems of scenario *2* by area for the purpose of constructing the .192 scenario. The J92 gridded balance map emphasizes melting inland of the Filchner-Ronne and Amcry Icc Shelves and places less emphasis on the melting of the narrow icc shelf systems girdling Antarctica,

Jacobs and Hellmer [1996] have recently updated the estimate of ice shelf melting to -*756* Gt/yr from -544 Gt/yr, based on new observations from the southern Amundsen and Bellingshausen Seas. This moves the total Antarctic icc sheet balance from -469 to -681 Gt/yr, placing it even more firmly negative, and would require only 25°A of the imbalance to comc from grounded portions of the ice sheets to account for the IPCC shortfall.

The four scenarios described in detail here include the three Antarctic scenarios discussed by *James and Ivins [1995]*. Scenarios 1 and J92 arc the same. Scenario 2 by mass is the same as *James and Ivins*' [1 99S] scenario 2. *James and Ivins [* 1995] did not discuss scenario 2 by area.

Additional Mass Balance Scenarios

In addition to the four Antarctic scenarios described above, wc will consider the global geodetic response to three other scenarios as follows: one for Antarctica, onc for Greenland, srnd onc accounting for mountain glaciers and small ice caps.

1'0 **scenario.** The T0 scenario (Figure 7a) shows *Trupin*'s [1993] steady-state Antarctic scenario with 0.0 mm/yr of sea level contribution. Trupin considered three scenarios of Antarctic ice mass change using *Radok et al.*'s [1986] gridded surface mass accumulation data files and, for each scenario, evaluated three cases corresponding to 0.0, 0.6, and 1.2 mm/yr of sca level fall. The steady-state scenario corresponds to the situation where a spatially uniform sheet of mass is removed from the accumulation rates to give the desired amount of sca level change.' Antarctic accumulation rates tend to be largest around the periphery; consequently, removing a uniform sheet of mass leads to mass loss in the interior and mass increase along the coast and in the Antarctic Peninsula.

Northeast Greenland. 10 Figure 7b a northeast Greenland scenario is shown that is a relatively ad hoc model constructed from the results of *Fahnestock et al.* [1993], who reported flow feat urcs reminiscent of Antarctic icc streams in northeastern Greenland based on satellite imagery. It was developed by assuming that the flow features correspond to a substantial mass loss in this region, large enough, in fact, to account for the missing mass equivalent to 0.4S mm/yr of sca level rise implied in the I I'('C report [*Warrick and Oerlemans, 1* 990]. With Greenland already assumed to bc providing 0.4 mm/yr, this assumption requires that Green land bc contributing approximately 0.4 + 0,45 = 0.85 mm/yr of sea level rise. As constructed, the scenario provides 0.91 mm/yr. The striking aspect of this scenario is that it alone explains nearly the entire observed polar motion signature. This scenario is not rooted in any glaciologically-derived mass balance studies and, consequently, should bc viewed as an interesting but entirely speculative demonstration case,

Mountain glaciers and small **ice caps**. A fairly well constrained scenario can be assembled for the mass changes of globally distributed mountain glaciers and small ice caps. *Meier* [1984] grouped mountain glaciers and small ice caps into 31 regions and, for 13 of these regions, determined long-term mass balances. He then employed a linear relation between annual mass balance amplitude and long-term (secular) mass balance to estimate secular mass balance for those regions where only annual mass balance amplitudes were known, We utilized Meier's mass balance estimates, whet-e available, and otherwise used the linear parameterization to determine secular mass balance for all 31 regions. Our gridded version of this global estimate corresponds to a 0.38 mm/yr contribution to sea level rise.

Computation of $\dot{J}_l$ and $\dot{\mathbf{m}}$

Low-degree, secular variations in the Earth's gravitational field $\dot{J}_l$ and the secular drift of the pole $\dot{\mathbf{m}}$ are sensitive to ongoing changes in surface mass loads. With sufficiently precise observations and by considering all likely global geodetic sources, constraints can potentially be placed on present day sea level sources [*Lambeck*, 1980; *Mitrovica and Peltier*, 1993; *Nerem and Klosko*, 1996]. } Iere we briefly review how secular global geodetic quantities may be obtained from a specified changing sLn face mass load.

The Earth's external gravitational potential field 4 can be expanded using normalized associated Legendre functions $\bar{P}_{lm}(\cos\theta)$

$$\phi(r,\theta,\lambda) = -\frac{Gm_e}{r}\left[1 + \sum_{l=2}^{\infty}\sum_{m=0}^{l}\left(\frac{a}{r}\right)^l \times \left\{\bar{C}_{lm}\, c_1(m\lambda) + \bar{S}_{lm}\, c_2(m\lambda)\right\}\bar{P}_{lm}(\cos\theta)\right]$$
$$= -\frac{Gm_e}{r}\left[1 + \sum_{l=2}^{\infty}\sum_{m=0}^{l}\sum_{j=1}^{2}\left(\frac{a}{r}\right)^l \bar{C}_{lmj}\, \bar{Y}_l^{mj}(\theta,\lambda)\right]. \qquad (1)$$

I let c we have int roduced the spherical harmonics $\bar{Y}_l^{mj}(\theta,\lambda)$, where c_1 and c_2 arc "cos" and "sin" functions, and O and λ arc colatitude and longitude, respectively. In (l), G is the gravitational constant; r? and m_e arc the Earth's mean radius and mass, respectively; while r is the radial distance from the Earth's center. The spherical harmonics arc normalized with a factor

$$N_{lm} = \left[\frac{(l-m)!\,(2l+1)\,(2-\delta_{0m})}{(l+m)!}\right]^{1/2}, \qquad (2a)$$

such that $\bar{P}_{lm}(\cos\theta) = N_{lm} P_{lm}(\cos\theta)$, and

$$\int_S \bar{Y}_l^{mj}(\theta,\lambda)\, \bar{Y}_{l'}^{m'j'}(\theta,\lambda)\, dS = 4\pi\, \delta_{ll'}\, \delta_{mm'}\, \delta_{jj'}\,. \qquad (2b)$$

The Stokes coefficients $\bar{C}_{lmj}$ arc given by

$$\bar{C}_{lmj} = \frac{a^2(1+k_l')}{m_e(2l+1)}\int_S \sigma(\theta,\lambda)\, \bar{P}_{lm}(\cos\theta)\, c_j(m\lambda)\, dS$$
$$= \frac{4\pi a^2(1+k_l')}{m_e(2l+1)}\,\sigma_{lmj} \qquad (3)$$

[*Chao et al.*, 1987], where $\sigma(\theta,\lambda)$ is the equivalent surface

mass density of an applied surface load rind the elastic load 1 .ove number is k_l^{el}. The surface mass density load consists of an applied ice load and corresponding ocean load. The ocean load is assumed to be uniformly distributed throughout the oceans and is chosen to render the total imposed surface mass equal to zero. Hence the global geodetic parameters computed here for present day ice mass changes include the eustatic ocean load correction [e.g. *Chao and O'Connor*, 1988a].

Analyses of satellite orbital element accelerations, from which time-varying gravity is a by-product [e.g., *Eanes and Bettadpur*, 1996], utilize unnormalized harmonics in expanding the Earth's zonal gravitational field

$$\phi(r,0) = -\frac{Gm_e}{r}\left[1 - \sum_{l=2}^{\infty}\left(\frac{a}{r}\right)^l J_l P_l(\cos 0)\right], \quad (4)$$

which, in light of the foregoing, gives

$$J_l = (2l+1)^{1/2}\bar{C}_{l0} = \frac{a^2(1+k_l^{el})}{m_e}\int_S \sigma(0,\lambda)P_{l0}(\cos 0)\,dS = \frac{4\pi a^2(1+k_l^{el})}{m_e(2l+1)}\bar{\sigma}_{l0} \quad (5)$$

where in (3) and (s), $\bar{\sigma}_{lmj}$ and σ_{lmj} arc the normed and unnormed spherical harmonic coefficients of a surface density load, respectively. From (5) it is clear that the gravitational coefficients J_l arc obtained from the surface mass or density load $\sigma(0,\lambda)$ through an integral with Legendre polynomial weighting functions, $P_l(\cos 0)$.

Perturbation of the Earth's inertia tensor through surface loading leads to changes in Earth rotation through conservation of angular momentum. Standard methodology involves writing the Earth's perturbed rotational state $\boldsymbol{\omega}$ referenced to the mean angular velocity of the Earth Ω; we have

$$\omega_1 = \Omega m_1; \quad \omega_2 = \Omega m_2; \quad \omega_3 = \Omega(1+m_3) \quad (6)$$

[*Lambeck*, 1980], where the standard axes $\mathbf{x}_1$, x_2, and $\mathbf{x}_3$ point in the direction of Greenwich, 90°E, and the (north) axis of rotation, respectively. The m_1 and m_2 are direction cosines of polar motion, Owing to the small angles involved, the $m_{1,2}$ can be viewed as the angles subtended by tbc x_1 and x_2 components of the perturbed rotation $\boldsymbol{\omega}$ and the X_3 axis. The time rate of change of polar motion $\dot{m}_{1,2}$ is therefore commonly expressed as the time rate of change of an angle, in milliseconds of arc per year (mas/yr) (1 radian = 2.063×10^8 mas).

Like the gravitational coefficients J_l, polar motion $\mathbf{m} = \dot{m}_1\mathbf{x}_1 + \dot{m}_2\mathbf{x}_2$ can be obtained directly from the specification of a surface mass load [e.g. *Lambeck*, 1980]. For a load that is changing at a constant rate, we have

$$m_j = -\frac{4}{5}\pi\frac{N_{21}a^4}{C-A}X_{woh}\,\bar{\sigma}_{21j} \quad (7)$$

[*Lambeck*, 1980]. The quantity $N_{21} = (5/3)^{1/2}$ is the degree 2, order 1 normalizing coefficient. The transfer function X_{woh} is given by the product of $k_0/(k_0 - k_2)$, which accounts for changes in the centrifugal potential ($k_0 \approx 0.942$ and $k_2 \approx 0.30$ is the degree 2 tidal loading response), and $(1+k_2^{el})$, which accounts for the elastic yielding of the Earth ($k_2^{el} \approx -0.30$).

The quantities C and A are the polar and equatorial moments of inertia, respectively. The direction of polar wander γ (in a northern hemisphere perspective) is given by

$$\gamma_{NH} = \arctan(\dot{m}_2 / \dot{m}_1) \quad (8)$$

measured counterclockwise (eastward) from the Greenwich meridian. In a southern hemisphere perspective the direction of polar motion γ_{SH} is obtained by adding 01 subtracting 180° from γ_{NH}.

Polar Motion and Low Degree Gravitational Coefficients

This section discusses the polar motion $\dot{\mathbf{m}}$ and gravitational coefficient $\dot{J}_l$ predictions, The following section discusses global composite scenarios that include known sca level sources aod are constructed to provide $\dot{J}_l$ predictions that agree with observations.

Prediction of Polar Drift Signature

lateral movement of surface mass causes a corresponding shift in the principal moments of inertia of the Earth. In turn, this forces a shifting of the Earth's pole of rotation with respect to the fixed crust. The net effect of mass buildup is to cause tbc pole of rotation 10 move away from the mass. Spherical harmonic degree 2, order 1, sLIr'face mass density coefficients were obtained for each of the mass balance scenarios shown in Figures 6 and 7, and polar motion drift rates were thca determined using (7) and (8).

The polar motion results are summarized in Table 4, and the directions and magnitudes of polar motion are given in Fig ure 8 in both a northern and southern hemisphere perspective. Figure 8 confirms the above qualitative description; that is, Greenland is losing mass, and Figure 8b shows the pole moving, toward Greenland. Indeed, this scenario is remarkable in that it alone accounts for a substantial fraction of the observed drift of the pole. In the southern hemisphere (Figure 8a) the substantial mass lost inland of the Filchner-Ronne Ice Shelf in the J92 scenario is reflected in the direction of polar motion for that scenario.

The direction of polar motion for scenario 1 is a combination of motion away from Pine Island Glacier and motion toward the Riiser-Larsen Ice Shelf. The resultant polar motion points toward neither region, showing how various potential sources of polar motion may sum to provide a resultant vector that is not obviously related to any of the sources. For both scenario 2 by mass and scenario 2 by area, the mass increase in East Antarctica, even though it is distributed Over a large azimuthal range, dominates the mass increase of the Pine Island Glacier and (for scenario 2 by mass) the Antarctic Peninsula. Consequently, both predictions are in the approximate direction of 270°E. The polar motion due to small ice caps and mountain glaciers is relatively small, reflecting the longitudinal variability of the mass sources, as noted by *Peltier* [1988] and *Trupin et al.* **[1992],**

By far, the largest polar motion prediction is that for *Trupin*'s [1993] TO scenario. The predicted direction is caused by the mass increase in the Antarctic Peninsula, combined with the mass decrease that is concentrated in inland East Antarctica,

These two effects dominate over the coastal regions of mass increase in East Antarctica. The $\dot{m}$ values given by *Trupin* [1993] for his steady-state, 0.0 mm/yr sea level change scenario are compared to the T0 values computed bet-c in Table 4. Trupin's quoted polar motion magnitude $\dot{m}$ has been reduced by a factor of 1.12 because we do not include the possible effect of core coupling,. Agreement is fairly good, considering the differences that can arise in constructing this scenario.

The polar motion predictions for our four Antarctic scenarios are considerably smaller than the T0 prediction (and the other Antarctic scenarios considered by *Trupin* [1993]) and, at most (for the J92 scenario), attain 1/3 the magnitude of the observed secular polar motion, Although the polar motion arising from present clay Antarctic ice mass changes should probably be included in polar motion budgets, the effects may not be as large as previously indicated. However, any substantial hydrological imbalance of the Greenland ice sheet would be sufficient to excite significant polar motion because Greenland is located away from the rotation axis nearer a peak of the degree 2, order I, 1 egendre function.

Peltier and Jiang [1996] have most recently considered secular polar motion in the context of postglacial rebound and find that the observed secular polar motion can be explained in terms of postglacial rebound alone, if there is a substantial viscosity increase in the deeper portions of the lower mantle. Future polar motion analyses using more tightly constrained present day surface mass transport models are necessary. A full treatment might also include consideration of longer timescale phenomena such as mountain building [e.g., *Vermeersen et al.*, 1994] and should also address uncertainties in the determination of the observed secular polar drift. A comprehensive treatment of polar motion is beyond the scope of the present paper, and hereafter we shall limit the discussion to the zonal gravity harmonics,

Time-varying Zonal Gravity Coefficients

Zonal gravity coefficients represent the axially symmetric undulations of the external gravity field. The I = 2, m = O and l = 3, m = O coefficients have simple geometric interpretations, the former reflecting oblateness and the latter the Earth's axial pear shape. Although large nontidal J_2 and J_3 values can result from mantle rebound, they may also be driven by surface mass transfer such as the continent-ocean hydrological exchange that causes secular sea level rise. Figure 9a shows a tutorial example in which the Greenland ice sheet ablates and the grounded Antarctic ice sheet grows, causing a dominantly pole-to-pole mass exchange. Growth in both the pear shape (J_3) and higher odd-degree zonal harmonics must accompany this climate change scenario. This particular example would not produce a corresponding large J_2 since equatorial regions would only be indirectly involved and the oblate shape of the Earth would be little affected.

Zonal nodal structure. Figure 9b shows the weighting functions -1'1 (cos0) (equation (5)) for the zonal harmonics near the south pole. The zeroes (nodes) of degrees 2, 3, and 4 are located well outside Antarctica but approach Antarctica with increasing degree. The degree 5 node is located near the East Antarctic coastline, and for higher degrees the node is located well inside some parts of East Antarctica, illustrating, that with

increasing degree comes increasing sensitivity to the details of Antarctic mass redistribution. The alternation in sign between even and odd harmonics at the south pole (O mar 180°) **is** also apparent in Figure 9b. 1 egendre polynomials do not alternate near the north pole (O near 00), explaining why the $\dot{J}_l$ values of the Antarctic scenarios alternate in sign with increasing degree but the Greenland scenario $\dot{J}_l$ values do not (Table 5). For a uniform Antarctic icc mass increase ($\dot{\sigma} > 0$ in Antarctica), corresponding to a sca level fall, Figure 9 illustrates that $\dot{J}_2$ and $\dot{J}_4$ will be negative and $\dot{J}_3$ and $\dot{J}_5$ will be positive. This rule of thumb is gene tiny valid but breaks down if there is a strong latitudinal dependence to the pattern of Antarctic icc sheet ablation and growth such as is present in the T0 scenario, which features interior ablation and coastal growth. For higher degrees it becomes increasingly more important to know the location of the changing mass because the nodes are located within Antarctica.

$\dot{J}_1$ Magnitude. The computed $\dot{J}_l$ values tend to maintain their magnitudes to approximately degree 6, then decrease in size (T 'able 5). An exception is the mountain glaciers scenario, for which the magnitudes arc negligible for degree 4 and greater. This is presumably due to the wide variation in latitude of the mountain glaciers and ice caps, leading to relatively efficient cancellation. The T0 scenario features a marked increase in $\dot{J}_l$ magnitude with degree 1, With its mass loss in the interior and mass increase along the coastlines, the T0 scenario is well situated to contribute to the degree 7 and 8 harmonics, which change sign at about the same latitude in East Antarctica as dots the mass accumulation of the T0 scenario, Foi higher degrees (not sh own) the T0 $\dot{J}_l$ values decrease rapidly with degree /. 't'here is very good agreement between our calculated '1 0 $\dot{J}_l$ values and those given by *Trupin* [1993].

The sea level/$\dot{J}_1$ dependence for Antarctica. Figure 10 shows how the predicted $\dot{J}_l$ **values vary with sea level change for our four gridded scenarios and the Antarctic scenarios studied by** *Trupin [* **1** 993]. Each frame in Figure 10 shows the $\dot{J}_l$ predictions on the ordinate axis and the corresponding sca level change on the abscissa. For the lowest degrees there is a fairly good, linear relationship between sca level change and the predicted $\dot{J}_l$ values for our Antarctic scenarios **(solid** line; linear equation given above each frame). The linear fit degrades with increasing degree, and for degrees 6 and higher the fit is relatively poor. The magnitude of the y intercepts of the linear fits for our scenarios arc negligible at the lowest degi ccs and increase with degree. This reflects the tendency of the low-degree $\dot{J}_l$ harmonic to depend mainly on the total mass being gained oi lost, whereas the higher harmonics arc more sensitive to the spatial distribution of the mass change,

However, *Trupin*'s *[1993]* scenarios show it is possible to construct Antarctic scenarios with no net mass change but with substantial predicted $\dot{J}_l$ values, even at the lowest degrees (Figure 10; also sec Table 5 for the T0 scenario). In addition to the steady state scenario discussed above, from which the T0 scenario was obtained, Trupin considered the cases in which the interior is thinning at the surface mass accumulation rates given by *Radok et al.* [1986] and the exterior is thickening at the surface mass accumulation rates ("thinning interior") and the opposite case of interior thickening and exterior thinning ("thickening interior"). For these scenarios the boundary

between the interior and exterior regions was defined to be a surface mass accumulation contour line chosen to give the required amount of sea level change (0.0, -0.6, or -1.2 mm/yr). Although the slopes of the lines for *Trupin*'s [1993] scenarios are similar to ours at low degrees, they have markedly nonzero y intercepts, reflecting the much stronger variation of mass change with latitude for these scenarios. In the following section we will primarily employ the linear relationships developed from our scenarios, as they embody current knowledge of Antarctic ice sheet balance.

Global Composite Scenarios

Can global composite scenarios be constructed that satisfy observational constraints on $\dot{J}_l$ values, account for the various known $\dot{J}_l$ sources, and satisfy constraints on total sea level rise? To answer this, it is necessary first to determine the Greenland sea level/$\dot{J}_l$ dependence similar to that determined for Antarctica. As well, consideration must also be given to the $\dot{J}_l$ contribution from postglacial rebound, which is often parameterized in terms of mantle viscosity, assuming a given load history such as ICE-3G [e.g., *Ivins et al.*, 1993; *Mitrovica and Peltier*, 1993].

Sea Level/$\dot{J}_l$ Dependence for Greenland

Sea level/$\dot{J}_l$ parameterizations can be developed for Greenland in the same way as for Antarctica. Figure 11 is similar to Figure 10 and shows how Greenland $\dot{J}_l$ varies with its contribution to sea level change for *Trupin*'s [1993] two Greenland scenarios and our NE Greenland scenario. *Trupin*'s [1993] scenarios were derived from two gridded maps of Greenland surface mass accumulation rates given by *Radok et al.* [1982]. The two maps correspond to different assumptions about the location of the Benson line, which is the boundary between interior regions of net positive surface mass imbalance and peripheral regions of net negative surface mass imbalance. For the two cases, then, of an inner Benson (IB) and outer Benson (OB) line, *Trupin* [1993] subtracted uniform sheets of mass necessary to provide specified amounts of sea level rise (-0.5, -0.1, and 0.3 mm/yr).

Trupin's [1993] two scenarios give very similar $\dot{J}_l$ predictions as a function of sea level rise. These predictions are not dissimilar, in fact, at low harmonic degree, to the predictions of our NE Greenland scenario (see the solid line in Figure 11, produced by assuming that the NE Greenland $\dot{J}_l$ contributions are proportional to its contribution to sea level change).

In the following global composite scenario analysis, the average sea level/$\dot{J}_l$ dependence of *Trupin*'s *[1992]* two Greenland scenarios is assumed: $\dot{J}_2 = 37.4\dot{\xi}_G$, $\dot{J}_3 = 34.2\dot{\xi}_G$, $\dot{J}_4 = 30.9\dot{\xi}_G$, and $\dot{J}_5 = 20.1\dot{\xi}_G$, where $\dot{\xi}_G$ is the Greenland contribution to sea level change (see Figure 11). The act Greenland sea level/$\dot{J}_l$ dependence seems to be relatively unimportant. Preliminary global scenario analyses incorporated the rather ad hoc NE Greenland scenario rather than the average of Trupin's scenarios, and there was no significant change in the overall patterns.

Rebound Calculations

The glacial rebound contribution depends on the assumed ice load history, which is highly uncertain in Antarctica, as well as mantle viscosity. Therefore the composite scenarios derived in this section should be viewed as illustrative and not definitive, as will be discussed further in the final section. Figure 12 shows predicted $\dot{J}_l$ values for two different parameterizations of lower mantle viscosity with the difference occurring in the treatment of viscosity variations in the deepest 650 km of the lower mantle (2235. S to 2885.5 km depth). The solid lines are *Mitrovica and Peltier*'s [1993, Figure 1] predictions with mantle viscosity varying beneath 670 km depth. The dashed lines correspond to *Ivins et al.*'s *[1993]* calculations, in which mantle viscosity also varies beneath 670 km depth, but the deepest 650 km of the lower mantle are held at a constant, relatively high viscosity of 6×10^{23} Pa s. The latter parameterization follows from the tendency of full numerical convective simulations to maintain a fairly thick high viscosity notch above the bottom thermal boundary layer [*Christensen*, 1985; *Ivins et al.*, 1993; *Tackley*, 1996]. *Pari and Peltier* [1995] have given a recent summary of all geodynamical constraints on the viscous profile of the mantle, in which they also favor the existence of a deep high viscosity notch. in both cases the ICE-3G loading history [*Tushingham and Peltier*, 1991] is used and the upper mantle viscosity is assumed to be 10^{21} Pa s. In the following we will refer to the *Mitrovica and Peltier* [1993] calculations as the homogeneous lower mantle (HIM) case and the *Ivins et al.* [1993] calculations as the 650-km boundary layer (650BL) case,

For a fairly wide class of late Pleistocene deglaciation models the prediction of time rate of change in the Earth's shape $\dot{J}_l$ shows a prominent peak in the response when plotted as a function of lower mantle viscosity, a feature that was first pointed out by *O'Connell* [1971]. Peak $\dot{J}_l$ rates occur at viscosity values that are small enough to respond fully to the loading, cycle, yet large enough that there is still a substantial ongoing response at present. Viscosities that are too small have almost completely returned to a state of gravitational equilibrium and hence give small present day rates. in contrast, an extremely high lower mantle viscosity produces a response that is too "sluggish".

Shown in Figure 12 is the observed $\dot{J}_2$ value obtained by *Nerem and Klosko* [1996], It is clear that if glacial rebound were the only process contributing to the nontidal time rate of change of the degree 2 gravitational field, there would be two preferred values for the viscosity that explain the observations [e.g., *Peltier, 1983]*. It will be shown in the analysis presented below, wherein we incorporate the effect of ongoing sea level change, that this duality in the mantle viscosity solution is a rather enduring feature.

The most striking difference between the two sets of curves is the shift of peak $\dot{J}_l$ values to smaller mantle viscosities for the 650BL case. The shift to smaller mantle viscosities occurs because the presence of the high-viscosity 650-km thick layer renders the "average" lower mantle viscosity higher than in the homogeneous lower mantle case. That is, a given viscosity in the zone above the boundary layer produces behavior like a somewhat higher viscosity applied across the whole lower mantle. The magnitude of the shift decreases with increasing degree because higher-degree gravitational coefficients sample

less deeply into the lower mantle [*Mitrovica and Peltier, 1991].*

Baseline Assumptions for Global Composite Scenarios

That present day hydrological transfers between the polar ice sheets and ocean are an important source for $\dot{J}_l$ and must be simultaneously considered along with postglacial rebound has been known for some time [e.g., *Sabadini et al., 1988; Wahr et al.*, **1993]** and has most recently been discussed by *Nerem and Klosko [1996].* Our approach parallels that taken by the latter authors. A rough sketch of this type of analysis is given by *Lambeck* [1980, chapter **9],** and has also been discussed by *Mitrovica and Peltier [l 993].*

Wc systematically vary the assumed lower mantle viscosity and sca level change $\dot{\xi}$ sourced to the negative (or positive) mass balance state of both the Antarctic and Greenland ice sheets. The sum of the predicted $\dot{J}_l$ contributions from the various sources are then compared to the values deduced from satellite observations. We commence with seven basic assumptions to determine the general pattern of behavior, then examine the consequences of varying a number of the assumptions.

The assumptions arc as follows, (1) The postglacial contribution to $\dot{J}_l$ comes from either the ICE-3G or 650BP cases (see Figure 12). (2) The Antarctic $\dot{J}_l$ contribution can bc determined from the linear relationships between sea level and $\dot{J}_l$ given in Figure 10 for the four Antarctic scenarios developed in this study (solid line, see above each frame). (3) The Greenland $\dot{J}_l$ contribution depends oa the Greenland contribution to sea level change in a way specified by the mean slopes given by *Trupin*'s [*1993] two* Greenland scenarios (Figure 11, mean slope of short- and long-dashed lines; sec above each frame), (4) The sea level and J_l contributions from mountain glaciers and small ice caps are known (Tables 4 and 5 [after *Meier*, 1984]). (5) The thermal expansion contribution to sea level change is roughly 0.4 mm/yr [*Warrick and Oerlemans*, 1990]. (6) The anthropogenic effect on sea level change is negligible. (7) Other potential $\dot{J}_l$ sources are negligible.

Searches for optimal parameter combinations were undertaken for a number of choices of total sca level change $\dot{\xi}$. For each choice the Antarctic contribution was allowed to vary systematically. With thermal expansion accounting for 0.4 mm/yr of sea level rise and the melting of mountain glaciers and small icc caps providing an additional + 0.38 mm/yr, the Greenland contribution to sca level change and hence J_l could be determined.

As a measure of the quality of any particular fit, a normalized standard deviation

$$d = \left\{ \left[\sum_{l=2}^{4} \left[(\dot{J}_l^o - \dot{J}_l^p) / \sigma_l \right]^2 \right] / 3 \right\}^{1/2} \qquad (9)$$

was computed. Here the superscripts "o" and "p " refer to the observed and predicted values, respectively, and σ_l is the quoted uncertainty of the observation. This quantity is constructed to have tbc value 1 if tbc predictions, in a root-sum-square sense, are a distance of 1σ from the observations, a value of 2 if the predictions arc located 2σ from the observations, and so on.

Except where noted, wc usc the $\dot{J}_l$ determinations of *Nerem and Klosko* [1996] based on analysis of LAGEOS 1 and 2, Ajisai, and Starlette orhits as follows: $\dot{J}_2 = -27.7 \pm 2{,}5$,

$\dot{J}_{3I}$ = 15.7 ± 3.5, and $\dot{J}_4$ = 2.() ± 14.6 (in 10^{-22} yr^{-1}). The degree 3 determination is the lumped observation $\dot{J}_{3I} = \dot{J}_3 + 0.837\dot{J}_5$. Holding the predicted values $\dot{J}_I^p$ = O, the standard deviation of the observations is 6.9.

Self-consislcmq for the Viscosity Models

Figure 13 shows the contoured standard deviations when the postglacial $\dot{J}_I$ come from the homogeneous lower mantle (III .M) case, shown as solid lines in Figure 12. Results are shown for the total amount of sea level rise ranging from O to 2.5 mm/yr. Figure 13 clearly indicates that there arc. choices of the somewhat ambiguous observation of total ongoing sea level change $\dot{\xi}$, Antarctic sourcing for sca level change $\dot{\xi}_4$, and lower mantle viscosity that cause the standard deviation to bc substantially reduced below the standard deviation of the observations ($\approx$ 6.9). Across a range of total sca level rise $1 \leq \dot{\xi} \leq 2$ mm/yr there are parameter choices that reduce tbc standard deviation to less than 1.0.

Aiso clearly shown in Figure 13 arc the well-known low and high viscosity solution branches characteristic of late Pleistocene rebound models. Along these branches the standard deviation is reduced in a similar style. The two branches appi each onc another with increasing $\dot{\xi}$ and, indeed, merge at $\dot{\xi}$ = 2.0 mm/yr with a lower mantle viscosity of 2 x 10^{22} Pa s. As total sca level rise $\dot{\xi}$ increases above 2.0 mm/yr, the minimum standard deviation increases substantially, producing a value d = 4.2 at $\dot{\xi}$ = 2.5 mm/yr (which is near the largest recent estimate of present day eustatic sca level rise). As $\dot{\xi}$ decreases below 1.0 mm/yr, tbc branches diverge farther. The high viscosity branch disappears beyond 10^{23} Pa s at 0.5 mm/yr total sca level rise, whereas the low viscosity branch has a pronounced standard deviation minimum of 1.33 (lower mantle viscosity is then 10^{21} pa s with Antarctica's sourced contribution $\dot{\xi}_4$ = -0. I mm/yr). At $\dot{\xi}$ = 0.0 mm/yr, the viscosity of the low-viscosity branch minimum is reduced to less than 10^{21} Pa s.

Figure 14 shows a similar analysis for the 650-km boundary layer (650111.) postglacial rebound case. *Ivins e/ al.*'s [1 993] calculations assume an ICE-3G loading history, a lower mantle viscosity that varies from 1 02(' to 10^{23} Pa s, and that the deepest 650 km of lower mantle is fixed at 6 $\times 10^{23}$ Pa s. The broad features arc similar to the III.M case, with two branches of solutions that are widely separated at $\dot{\xi}$ = 0.0 mm/yr and that approach onc another with increasing total sca level rise $\dot{\xi}$. In detail, the behavior is somewhat different. The preferred lower mantle viscosity values arc smaller by a factor of 5 to 10 when compared to the III.M case. The two branches merge at 2.5 mm/yr of total sca level rise rather than 2.0 mm/yr.

Toward a Constraint on Present-day Antarctic Mass Balance?

l'able 6 defines 11 global composite scenarios, based on the location of the standard deviation minima in Figures 13 and 14. For both the I II.M and 650BI cases it shows a relation between total sca level change and the location of the minimum standard deviation, For $\dot{\xi}$ = 1.0 mm/yr, Antarctica ablates at a rate that contributes roughly $\dot{\xi}_4$ = 0.2 mm/yr to that total rise rate. As the total assumed sca level rise $\dot{\xi}$ increases to 2.0-2.5 mm/yr, the Antarctic positive sourcing increases to about $\dot{\xi}_4$ =

0.8 to 1.0 mm/yr.

Table 7 shows the predicted and residual $\dot{J}_l$ values for the 11 composite scenarios. Postglacial rebound tends to produce the largest $\dot{J}_l$ signatures. The Antarctic mass balance signature is, generally, predicted to be the second largest and of opposite sign to the glacial rebound contribution. 'There is a trade-off between the contributions from rebound (which depends on mantle viscosity) and Antarctic mass balance (which depends on the Antarctic contribution to sea level change). For the ICE-3G case a lower mantle viscosity near 10^{22} Pa s (e.g., composite scenario D) predicts a large postglacial rebound $\dot{J}_l$ value. The latter therefore requires a large $\dot{\xi}_A$ to provide a large offsetting $\dot{J}_l$ contribution from Antarctica in order to match the observed $\dot{J}_l$ values. In comparison, the 650BL case has peak postglacial rebound $\dot{J}_l$ values around 2×10^{21} Pa s, corresponding to composite scenario J, which features 1.3 mm/yr of sea level rise from Antarctica. For both mantle viscosity parameterizations, then, a very substantial glacial rebound signal appears to be quite viable but implies a large amount of total sea level rise $\dot{\xi}$ and corresponding large negative mass balance for Antarctica.

From Table 7 the residual values tend to be largest for degree 4, a consequence of the J_4 value having the largest uncertainty. As we shall see, tighter observational constraints on J_4 are useful in reducing the range of allowable parameters that satisfy the $\dot{J}_l$ observations.

The $\dot{J}_l$ Budget

The general pattern shown in Figures 13 and 14 is robust. We varied a number of assumptions and found that the double-root solutions that merge with increasing, global sea level are quite persistent. To assist in understanding how varying a given source parameter can affect the location of the standard deviation minima, here we derive a formal expression for the $\dot{J}_l$ budget. The following development also highlights an important contrast in the constraints provided by even- and odd-degree harmonics.

For the purposes of our parameterization the total eustatic sea level change $\dot{\xi}$ is

$$\dot{\xi} = \dot{\xi}_A + \dot{\xi}_G + \dot{\xi}_M + \dot{\xi}_W, \tag{10}$$

where the subscripts A, G, M, and W refer to the sea level contributions from Antarctica, Greenland, mountain glaciers and small ice caps, and thermal expansion effects, respectively. The J_l contributions from Antarctica and Greenland, respectively, can be written as

$$\dot{J}_{lA} = a_l \dot{\xi}_A + b_l, \tag{11a}$$

$$\dot{J}_{lG} = c_l \dot{\xi}_G. \tag{11b}$$

The coefficients a_l, b_l, and c_l are the coefficients relating sea level contribution to J_l (e.g., see Figures 10 and 11), and for simplicity, we shall assume that the Greenland sea level/J_l dependance does not have a constant term. Relation (10) allows the Greenland contribution to sea level $\dot{\xi}_G$ to be eliminated from (11b), such that

$$\dot{J}_{lG} = c_l(\dot{\xi} - \dot{\xi}_A - \dot{\xi}_M - \dot{\xi}_W). \tag{12}$$

The total $\dot{J}_l$ budget is

$$\dot{J}_l = \dot{J}_{lA} + \dot{J}_{lG} + \dot{J}_{lM} + \dot{J}_{lPGR}, \quad (13)$$

where PGR refers to the postglacial rebound component. With (11a) and (12), this total can be rewritten as

$$\dot{J}_l = \dot{\xi}_A(a_l - c_l) + c_l\dot{\xi} \quad (14)$$
$$c_l(\dot{\xi}_M + \dot{\xi}_B) + b_l + \dot{J}_{lM} + \dot{J}_{lPGR}$$

If we assume that a parameter combination has been found that satisfies a set of observed $\dot{J}_l$, then (14) can be used to determine how a change to one of the source parameters forces another source parameter to change to maintain agreement with the $\dot{J}_l$ observations.

Equally important, (14) shows that the $\dot{J}_l$ budget depends on the Antarctic contribution to sea level $\dot{\xi}_A$ through the difference of the linear coefficients $a_l - c_l$. As a comparison of Figures 1(1 and 11 shows, the linear coefficients tend to be of the same size and sign for the even-degree harmonics, especially at degrees 2 and 4, so that the difference $a_l - c_l \approx 0$. This implies a lack of sensitivity of the even-degree $\dot{J}_l$ budget to the Antarctic contribution to sea level $\dot{\xi}_A$. In marked contrast, the linear coefficients for the odd-degree harmonics are of opposite sign and of approximately the same size, especially at degree 3, so that the difference $a_l - c_l \approx 2a_l$. Hence the odd-degree budget is twice as sensitive to the Antarctic contribution to sea level $\dot{\xi}_A$ as it is to the total sea level $\dot{\xi}$, whereas the even-degree budget is relatively insensitive to the Antarctic contribution to sea level. For degrees 2 and 3 we therefore have

$$\dot{J}_2 = a_2\dot{\xi} - a_2(\dot{\xi}_M + \dot{\xi}_W) + b_2 + \dot{J}_{2M} + \dot{J}_{2PGR}, \quad (15a)$$

$$\dot{J}_3 = 2a_3\dot{\xi}_A - a_3\dot{\xi} + a_3(\dot{\xi}_M + \dot{\xi}_W) + b_3 + \dot{J}_{3M} + \dot{J}_{3PGR}, \quad (15b)$$

with approximations $a_2 \approx c_2$ and $a_3 \approx -c_3$.

As an example of how (15) can be used, let us consider that we have found a parameter combination that satisfies observed $\dot{J}_l$ values; that is, we are located at a standard deviation minimum (a global composite solution). To remain at that standard deviation minimum, a change to one source parameter must be accompanied by opposite changes to one or more of the other parameters so that the left-hand-sides of (15a) and (15b) remain unchanged ($\delta\dot{J}_2 = \delta\dot{J}_3 = 0$). Let us assume that the thermal expansion of the oceans $\dot{\xi}_W$ is doubled from 0.4 to 0.8 mm/yr ($\delta\dot{\xi}_W = 0.4$ mm/yr). If we keep the mountain glacier and glacial rebound contributions unchanged ($\delta\dot{\xi}_M = \delta\dot{J}_{lM}, \delta\dot{J}_{lPGR} = 0$), then in (15a) the only way to offset the effect of the increase in thermal warming is to increase the global sea level rise $\dot{\xi}$ by an equal amount. The degree 3 relation (15b), with $\delta\dot{\xi} = \delta\dot{\xi}_W = 0.4$ mm/yr, is immediately satisfied without requiring a further change to another source parameter (such as Antarctic contribution to sea level). We conclude that the effect of increasing the thermal expansion is to shift the solutions toward larger amounts of global sea level rise but otherwise leave the solutions essentially unaltered. This is confirmed in the following discussion.

Although this example is relatively straightforward, in general, it is not obvious how perturbing a given source parameter affects the other source parameters. Consequently, through direct numerical calculation we varied the observational constraints to reflect other groups' $\dot{J}_l$ determinations, assumptions

regarding anthropogenic and steric effects on sea level rise and the mountain glacier $\dot{J}_1$ and sea level contributions, and the assumption that only surface loading contributes to $\dot{J}_1$, to see how the global composite solutions are affected. We found that the double branch of the viscosity solutions is a rather enduring feature.

To illustrate this, Figure 15 shows the trace of the standard deviation minimum when a variety of assumptions are varied, Figure 15 (left) shows how the location of the minimum standard deviation shifts as the total sea level change is varied, and Figure 15 (right) shows the actual values of the standard deviation d. The standard calculation against which the assumptions are varied is tied to the *Nerem and Klosko [1996]* satellite laser-ranging solutions for $\dot{J}_1$ and also relies on the ICE-3G postglacial rebound calculations (see list of assumptions and Figure 13).

Alternative Laser Ranging Solutions for $\dot{J}_1$. Figures 15a and 15b indicate the effect of using alternative $\dot{J}_1$ determinations, in addition to *Nerem and Klosko*'s [1996] values (solid line), we utilized *Cazenave et al.*'s *[1996]* values (short-dashed line) and *Cheng et al.*'s [1989] values (long-dashed line), shown in Table 8. Different groups pursued different data reduction strategies, so that *Nerem and Klosko* [1996] present a "lumped" $\dot{J}_{3l}$. $\dot{J}_3 + 0.837)_5$, whereas *Cheng et al.* [1989] and *Cazenave et al.* [1996] solve for an isolated $\dot{J}_3$.

Results generated by assuming either *Nerem and Klosko*'s [1996] or *Cheng et al.*'s [1989] values are actually quite similar. This can be attributed to the similarity of the respective solutions for $\dot{J}_2$ and $\dot{J}_4$ and further implies that Nerem and Klosko's lumped $\dot{J}_{3l}$ does not give an appreciably different constraint than Cheng et al.'s $\dot{J}_3$. The main difference is the markedly higher standard deviations obtained for the low-viscosity branch using Cheng et al.'s values. Examination of the residuals shows that it is the appreciably tighter constraint on Cheng et al.'s $\dot{J}_4$ that leads to the higher standard deviation along the low-viscosity branch. This shows how tighter constraints on higher-degree harmonics could assist in discriminating between competing, composite scenarios.

The only significant difference in the location of the standard deviation minima shown in Figure 15a is that the preferred solutions for *Cazenave et al.*'s [1996] $\dot{J}_1$ are systematically shifted toward higher Antarctic sea level contributions by 0.2 to 0.3 mm/yr. *Cazenave et al.* [1996] find a large negative value for $\dot{J}_3$. Satisfying this constraint would require an increase in Antarctic ice sheet ablation, in comparison to the other $\dot{J}_l$ solutions. The physics involved in this effect is explained in Figure 9a, although the sign and direction of the $\dot{J}_3$ and the hemispheric mass transport are reversed. This can also be understood by considering (15b), where, with $\delta\dot{J}_3 < 0$ and $a_3 < 0$ and all the source parameters fixed except for Antarctic contribution to sea level, we must have the change to the Antarctic contribution to sea level $\delta\dot{\xi}_4 > 0$.

Figure 15b shows that the standard deviation minima are typically below 2, except for *Cheng et al.*'s [1989] low viscosity branch. For all three sets of solutions the standard deviation is reduced to values of 1 or less for some combination of parameters. The smallest standard deviations (best fits) tend to be attained on the high-viscosity branch or where the two branches merge at 2×10^{22} Pa s.

Some Alternative Source Assumptions. In the foregoing analysis we assumed that the anthropogenic contribution to sea level is nil, that thermal expansion provides **0.4** mm/yr of sea level rise [*Warrick and Oerlemans*, 1990], and mountain glaciers provide 0.38 mm/yr [*Meier, 1984]*. There is uncertainty regarding the magnitude of all these effects. For example, *Meier* [1993] places the anthropogenic contribution to sea level at 0.23 ± 0.24 mm/yr, +0.06 to + 0.3 mm/yr caused by groundwater "mining" and -.07 to -0.17 mm/yr due to reservoir impoundment, obtained by adding the small estimate of reservoir impoundment to the larger estimate of groundwater depletion. However, if *Chao*'s [1995] recent estimate of -0.3 mm/yr for reservoir impoundment is accepted, then the anthropogenic contribution drops back to O or even becomes slightly negative. Similarly, a recent reassessment of the sterically induced rise Component of 0.22 to 0.s 1 mm/yr [*de Wolde et al.*, 1995] ranges from 50% to 120% of the value of 0.4 mm/yr adopted here [*Warrick and Oerlemans*, 1990]. Finally, *Trupin et al. [1996],* in considering the mass balance of mountain glaciers in western Canada and Alaska, argues that these glacier systems alone are contributing to sea level at a rate of 0.4 ± 0.2 mm/yr, which, if correct, suggests that *Meier*'s [1984] mountain glacier and small ice caps estimate is too small.

To address the uncertainty in these sources, and without attempting to determine "preferred" alternatives, we consider variations in the thermal expansion and mountain glacier sources. Figures 15c and 15d show the effect of assuming that thermal expansion contributes 0.8 mm/yr to sea level rise rather than 0.4 mm/yr (short-dashed line) and the effect of assuming that mountain glaciers contribute twice as much to sea level rise (0.76 mm/yr rather than 0.38 mm/yr) and, consequently, drive J_1 values that are doubled (long-dashed line). The effect of the doubled mountain glacier contribution is rather negligible; the curve is shifted down by a mere O. I mm/yr in Antarctic contribution to sea level. in contrast, as predicted in the discussion following (15a) and (15b), the dominant effect of doubling thermal expansion is to shift the solutions toward larger amounts of global sea level rise. The standard deviations again are typically less than 2, although for the doubled mountain glacier scenario the standard deviation dots not drop below unity for any combination of parameters. The important result is that perturbing these sources by a factor of **2 dots** not alter the general pattern of preferred global solutions.

A more profound effect is shown in Figures 15e and 15f, where the Antarctic sea level/$\sim_1$ parameterization is derived from *Trupin*'s [1993] steady state scenario, rather than from our gridded Antarctic scenarios. The steady state scenario features a strong latitudinal contrast between interior regions of mass loss and coastal regions of mass accumulation (the T0 scenario shown in Figure 7a is a specific instance of the steady state scenario corresponding to 0.0 mm/yr of Antarctic contribution to se? level). Although the slopes of the steady state sea level/.1, parameterizations (see the long-dashed lines of Figure IO) are quite similar to the slopes of our parameterizations, the steady-state parameterizations feature strongly nonzero intercepts. As shown in Figures 15e and 15f, this drives the global solutions toward significantly smaller amounts of total sea level rise and smaller amounts of Antarctic contribution to sea level.

The importance of this example is apparent when one recalls that the unmeasured areas described by *Bentley and Giovinetto* [1991] (*see* Figure S) all lie along the Antarctic coast. If future mass balance measurements along the East Antarctic coast reveal a strong contrast with interior regions, then the constant terms (the b_l term in 11a) in the Antarctic sea level/$\sim_l$ parameterizations would become nonzero, which would result in changes to the global composite scenarios, However, the size of the change would likely be smaller than that found for the steady state scenario unless the imbalance is much greater than that featured in scenario 2 by mass. Scenario 2 by mass, which provides -1. I mm/yr of sea level rise, has its extrapolated mass imbalance concentrated in coastal regions, and yet for low harmonic degrees it lies quite close to our nearly zero intercept parameterizations (solid lines, Figure 10). This indicates that much larger latitudinal mass balance contrasts are needed to obtain parameterizations with markedly nonzero intercepts.

Figures 15e and 15f also show the effect of assuming a contribution to the observed $\dot{J}_2$ from core flow-induced variations in the pressure field at the core-mantle boundary with magnitude $\dot{J}_2 = -13 \times 10^{-12}$ /yr [*Fang et al.*, 1996], a value about 1/2 of the observed $\dot{J}_2$. The estimate of the secular change in CMB pressure is somewhat speculative since it relies on the hypothesis of a frozen-flux field that is embedded in a nearly geostrophic core surface flow that is properly inverted for by employing geomagnetic field data spanning epochs 1965 to 1975 [see]; Bloxham *et al.*, 1989]. Here we include this estimate since it speaks, in some measure, to the question of how a fractional and possibly unmodelable part of observed $\dot{J}_2$ might corrupt our analysis. While the overall pattern is unchanged over much of the lower mantle viscosity range, the inclusion of the secular variation in CMB pressure does degrade the solutions and this is reflected in the higher standard deviations (poorer fit) over most of the viscosity range (Figure 15f). This degradation could be interpreted in the following four possible ways: (1) *Fang et al.* [1996] have overestimated the magnitude of the core-flow pressure effect, (2) there are yet other processes contributing to the secular variation of the global gravity field (such as internal oceanic and atmospheric mass exchanges), (3) either or both the parameterizations for the present day surface mass change and glacial rebound could be seriously in error, or (4) that all sources have been included and all the estimates and parameterizations are correctly considered, implying (from Figure 15f) that total sea level change is currently around 2.5 mm/yr and the "average" lower mantle viscosity is around 2×10^{22} Pa s. It would be premature to exclude any of these possibilities.

The Important Role of a Well-determined Odd-degree Secular Harmonic. As discussed above, an odd-degree harmonic constraint is needed to determine the Antarctic. (or Greenland) contribution to sea level. This crucial point is illustrated in Figure 16, which shows the contoured standard deviation obtained using *Eanes and Bettadpur*'s [1996] $\dot{J}_2$ and $\dot{J}_4$ values (Table 8), but excludes a constraint on $\dot{J}_3$. For a given amount of total sea level change the standard deviation is almost completely independent of the Antarctic contribution to sea level change. This occurs because the Antarctic and Greenland sea level/J_l parameterization for the even, low-degree harmonics is approximately equal; so as the Antarctic contribution

to sca level rise changes, Greenland's also changes but with opposite sign, and the two $\dot{J}_l$ contributions nearly cancel. What is left is the strong dependence on mantle viscosity. In marked contrast, if odd-degree harmonics arc included, with their opposite hemispheric parity, a tight constraint on the partitioning of sca level change sourced to the Antarctic and Greenland icc sheets is introduced. The tutorial example of Figure 9a also illustrates this.

The pronounced degradation in source constraint revealed in Figure 16 is caused by the assumed lack of knowledge of the secular variation of the Earth's skew-symmetric (odd /) harmonics. The latter harmonics have opposite parity to those of even / and the stark contrast of nonconvergent (Figure 16) to convergent standard deviation minimizations (Figures 13 and 14) is, indeed, a testament 10 their powerful information content. Polar sources of secular sca level variation arc constrained by low-degree secular gravity only if odd-degree constraints arc included,

Discussion and Summary

The global composite scenarios developed in this paper illustrate the powerful constraints on present day mass balance and 1 :arth rheology that a consistent, well-determined set of $\dot{J}_l$ observations could provide. 1 lowever, with the present large observational uncertainties for all but the relatively well-determined degree 2 harmonic, it cannot ycl bc argued that they provide definitive answers. Therefore efforts to improve observed secular zonal gravitational harmonics arc quite warranted.

Some portion of the observed secular polar motion may bc driven by the present day mass imbalance of Greenland or Antarctica [*Trupin*, 1993]. However, the signatures predicted here from the drainage basin [*Bentley and Giovinetto, 1991]* and icc shelf melt rate modified scenarios [*Jacobs et al.*, 1992] have a magnitude that is, at best, onc third of that observe.d, It would appear that a robust observation of $\dot{J}_3$ might provide a more important piecc of global geodetic information for con. straining Antarctic mass balance than does polar motion, Naturally, if the odd-degree harmonics arc to provide definitive constraints on polar icc mass balance, other possible sources for $\dot{J}_3$ (and higher degrees) must bc more tightly constrained, For example, a complete evaluation of the last half century of anthropogen ic-related hydrologic balance remains somewhat ambiguous and only the reservoir component appears to have been treated adequately [*Chao*, 1995].

Global Implications of the Antarctic Scenarios

Our gridded Antarctic scenarios arc based upon mass balance analyses of individual icc drainage basins [*Giovinetto and Bentley*, 1985; *Bentley and Giovinetto, 1991]*. The scenarios capture several important features of glaciologically and oceanographically based models. in particular, since they focus on individual drainage systems, they represent a common standard from which all types of acc umulation, flow, and ablation data arc to bc referenced in future data-based model improvements [e.g., *Bentley*, 1995]. Additionally, tbcy represent alternative cnd-member extrapolations to regions having little or no data coverage. As data that further constrain mass balance of

individual drainage basins become available, models based on this data will provide independent bounds on the Antarctic ice sheet contribution to observed $\dot{J}_l$ and $\dot{\xi}$. For example, recent reappraisals move the Pine Island Glacier toward a less positive mass balance [*Lucchita e/ al.*, 1995] and nearby ice shelves toward greater melting [*Jacobs and Hellmer*, 1 996], suggesting that a future round of scenario revisions might feature a less negative (more positive) Antarctic contribution to sea level.

Owing 10 the wide variation in $\dot{\xi}_A$ anti $\dot{J}_l$ that our models prodict, wc cannot argue that any onc of the four scenarios elaborated upon here necessarily represents a significant refinement over the scenarios used in previous studies by *Trupin* [1993] and *Mitrovica and Peltier [1993]* to determine mass balance related $\dot{J}_l$. 1 lowever, despite the differing ways in which mass imbalance was extrapolated to unmeasured regions, our Antarctic scenarios reveal a nearly linear relationship between the simultaneously predicted low-degree $\dot{J}_l$ and Antarctica's contribution to present day sca level change $\dot{\xi}_A$. Unless future scenario revisions include quite drastic changes from the current state of knowledge of Antarctic ice mass balance, tbc sea level/,), parameterizations developed from our models may prove to be relatively stable,

With similar linear relationships developed for Greenland sea level sourcing $\dot{\xi}_G$ and $\dot{J}_l$, this permits an exhaustive exploration to find optimum values of Antarctic and Greenland sea level sourcing that provide agreement with observed sea level and $\dot{J}_l$ when combined with other sca level and $\dot{J}_l$ contributors. Our search for optimum parameter combinations included assumed known sca level contributions from ocean thermal expansion and small icc masses and $\dot{J}_l$ contributions from small ice masses and glacial rebound. Lower mantle viscosity was freed as a parameter for the postglacial rebound $\dot{J}_l$, and the ICE-3G glacial load history of *Tushingham and Peltier [1991]* was assumed.

Numerous viable combinations or global composite scenarios of Antarctic and Greenland sea level sourcing and lower mantle viscosity could be found that satisfy observed $\dot{J}_l$ for global sca level rise $\dot{\xi}$ 1 tinging from less than 1 to 2-2,5 mm/yr. Postglaciai rebound is generally the largest $\dot{J}_l$ source for the composite scenarios. A well-known feature of postglacial rebound $\dot{J}_l$ is the existence of a pronounced peak at some lower mantle viscosity, implying, in general, the existence of two mantle viscosity solutions that can deliver a given postglacial rebound .),. The duality of $\dot{J}_l$-derived mantle viscosity solutions has been discussed at length [e.g., *Yoder et al.*, 1983; *Peltier*, 1983; 1985; *Rubincam, 1984; Yuen and Sabadini, 1985; Yuen et al,,* 1 986; *Mitrovica and Peltier*, 1989, 1 993; *Ivins et al.*, 1993; *Wahr et al.*, i 993], and wc found it to be a persistent feature of the global composite scenarios. However, the strong interrelationship between assumed total sea level rise $\dot{\xi}$ and the preferred 10WCI mantle viscosity revealed by the global composite scenarios has not previously been explicated.

in general, the two viscosity branches arc separated by a factor of 50 or more in mantle viscosity for total sca level rise around $\dot{\xi}$ = 1 mm/yr, and as $\dot{\xi}$ increases to 2-2.5 mm/yr the two branches approach one another and merge, For larger amounts of total sca level rise the solution degrades rapidly. This is entirely consistent with tide gauge analyses showing that total sca level rise is between I and 2.5 mm/yr, but it dots not

provide a new constraint. The largest contributor to $\dot{J}_l$ is post glacial rebound and is offset by a smaller Antarctic contribution of opposite sign. The secular variations in gravity harmonics driven by the Greenland ice cap, temperate glaciers, and other small ice caps tend to give a smaller contribution to the total.

The general pattern of the solutions was preserved in two very different parameterizations of lower mantle viscosity, one which assumed a homogeneous lower mantle (HLM) and another which assumed viscosity varying in the lower mantle but with the deepest 650 km fixed at a relatively high value of 6×10^{23} Pa· s (650HL). The effect of having a high-viscosity lower mantle is that the preferred viscosity of the remaining lower mantle is reduced relative to the HLM case. Both types of lower mantle viscosity structure provide rather nicely isolated solutions, and this tends to indicate that there exists a broad range of lower mantle viscosity stratifications capable of giving agreement with the observed $\dot{J}_l$ for a given choice of total sea level rise $\dot{\xi}$. When *Cheng et al.*'s [1989] $\dot{J}_l$ solutions were used, which feature a substantially smaller error estimate for $\dot{J}_4$ than the other laser-ranging solutions, a marked degradation in the fit of the low-viscosity branch solutions occurs. This suggests that in the future a tighter set of constraints on observed $\dot{J}_l$ for $l > 2$ might permit certain lower mantle viscosity structures to be excluded [*Mitrovica and Peltier*, 1991; *Ivins et al.*, 1993].

Provided the odd-l constraints are retained, the general character of the preferred solutions holds, even when some underlying assumptions are varied. Doubling the mountain glacier (and doubling their contribution to $\dot{J}_l$) or doubling the steric component of sea level rise only causes the preferred solutions for Antarctic sources to change slightly and has little effect on the glacial rebound dominated behavior. When the Antarctic sea level/, pat ameterizat ion is changed to reflect the strong latitudinal dependance of mass balance found for *Trupin*'s [1993] steady state scenarios, a larger change is observed, although again the basic solution behavior is retained. A case where about 1/2 of the observed $\dot{J}_2$ is assumed to come from processes other than glacial rebound or present day hydrological exchanges (specifically, pressure loading at the CMB predicted by *Yang et al.* [1996]) reveals the same basic solution behavior, although there is a poorer fit over much of the viscosity or total sea level rise range.

Antarctic Sea Level Sourcing and Odd Degree Zonal Harmonics

Our $\dot{J}_l$-based solutions for the sea level rise $\dot{\xi}_A$ caused by the mass imbalance of tile grounded Antarctic ice sheet tend to parallel the assumed total (global) sea level than.gc. The eustatic sea level components of the negative Antarctic mass balance solutions correspond to about, $\dot{\xi}_A = 0{,}0$ mm/yr at, $\dot{\xi} = 1{,}0$ mm/yr total sea level rise and to $\dot{\xi}_A = 1.0$ mm/yr at $\dot{\xi} = 2$ to 2.5 mm/yr. This requirement for Antarctic ablation is consistent with the assessment of large basal melting and calving rates in the Weddell Sea reported by *Jacobs et al.* [1992] and upon which the J92 scenario was constructed. The latter estimates are rather consistent with the observation that ice shelves at the margins of the Antarctic Peninsula, in both the Bellingshausen and Weddell Seas, have been retreating since about 1945 [*Vaughan and Doake*, 1996]. However, our estimates of

present day Antarctic sea level sourcing also depend critically on assumptions regarding the timing and magnitude of deglaciation.

For example, the global composite solutions change significantly when the glacial rebound $\dot{J}_l$ values of *Wahr et al.* [1993] (not discussed above) are used instead of the ICE-3G values of *Mitrovica and Peltier* [1993]. *Wahr et al.*'s [1993] calculations employ the same mantle viscosity structure as the ICE-3G case and only differ in assuming a simplified deglaciation history. Three disks, corresponding to the Laurentide, Scandinavian, and Antarctic ice sheets, which undergo steady, uniform glaciation and deglaciation phases peaking at 18 ka and ending at 8 ka, deliver peak glacial rebound $\dot{J}_l$ values which are only 50% or less of the peak ICE-3G values. This has a rather important effect on the global composite scenarios, as the range of acceptable total sea level rise drops to 0 to 1 mm/yr, and the corresponding range of Antarctic contribution to sea level is -0.4 to 0.3 mm/yr. This rather profound change shifts the global composite solutions from requiring Antarctic ablation (ICE-3G case) to allowing either Antarctic ablation or accumulation and highlights the importance of the deglaciation history in constructing secular renal gravity budgets.

It is therefore quite possible that changes to detailed deglaciation models such as ICE-3G could produce significant changes to .), -derived interpretations of mantle viscosity and ice mass balance. The ICE-3G model employed in all calculations here features a late (9-5 ka) Antarctic deglaciation, in marked contrast to models that feature an earlier southern hemispheric ice mass transfer to the ocean basins that is almost exactly in phase with the late Pleistocene and early Holocene northern hemispheric glacial retreat (e. g., ICE-2 [*Wu and Peltier*, 1983]). Shifting Antarctic deglaciation to earlier times would, in general, decrease the postglacial rebound $\dot{J}_l$ since the mantle has a greater time in which to reestablish gravitational equilibrium. The effect would be especially severe in the case of the skew-symmetric $\dot{J}_3$ because it depends on the difference between the northern and southern hemisphere deglaciations [*Yoder et al.*, 1983; *Ivins et al.*, 1993; *Mitrovica and Peltier*, 1993]. This would reduce the $\dot{J}_l$ values (relative to the ICE-3G case) in a manner similar in nature, if not in magnitude, to that described above for *Wahr et al.*'s [1993] $\dot{J}_l$ values. Consequently, we might expect that the ICE-4G model [*Peltier, 1994],* which features an earlier, smaller Antarctic deglaciation, would produce $\dot{J}_l$ values that would have to be compensated with smaller amounts of total sea level rise and smaller amounts of Antarctic ablation.

A main issue, and perhaps the most important result emerging from our study, centers around the size and sign of the lumped odd chain of harmonics. For example, a large negative value for $\dot{J}_3$ [*Cazenave et al.*, 1996] pushes the preferred solutions toward a global scenario having larger net Antarctic melt contribution to sea level rise at the expense of Greenland ice sheet ablation. Variation in even-/ harmonics (as reported in various analyses of satellite laser ranging data) affects the interpretation of Antarctic and Greenland sea level sourcing in a less sensitive manner, The sensitivity to the odd-/ chain is more dramatically exhibited in the preferred solutions when constraints on them are dropped entirely. in this case the dependence on Antarctic contribution to sea level nearly disap-

pears, and only mantle viscosity and the total sea level rise are important in determining preferred parameter combinations,

Estimates of J_3 and of the entire skew-symmetric (odd) chain could improve substantially with a more rigorous understanding of the nongravitational forces that affect high-orbit laser ranging satellites. For example, an impressive correlation between residuals in the orbital eccentricity element of LAGEOS 1 and the Earth's radiation (albedo) signature has been discovered recently by *Martin and Rubincam [1996]*. We conjecture that this indicates that a more robust, secularly varying pear shaped harmonic ($l = 3$) solution could soon be generated in analyses of satellite laser ranging data, This is needed if satellite-derived secular zonal harmonics are to contribute significantly to determining present day polar ice mass balance.

Acknowledgments. This research was supported by a NOAA Global Change Office grant, NASA grant NAGS- I 940, the i AGEOS 2 program, and the JPL Supercomputing Office. We thank Andy Trupin, Douglas Robertson, and Roger Bilham for reviews and Charlie Bentley and Stan Jacobs for comments that helped to substantially improve the original manuscript. Discussions with numerous persons, including Tony Lambert, Chuck Yoder, John Wahr, Dazhong } Ian, Charlie Bentley, Carol Raymond, Stan Jacobs, Steve Nerem, Steve Klosko, and Richard Eanes have clarified our ideas. in particular, we thank Andy Trupin for numerous discussions throughout the course of this research. Claire Hanson of World Data Center A and Nancy Greeley of the Cold Regions Research and Engineering Laboratory helped greatly with the Radok data sets. Many of the figures were generated with *Wessell and Smith*'s *[1991]* GM-1' software. Part of this work was performed at the Jet Propulsion Laboratory, California Institute of Technology, under contract with NASA, Geological Survey of Canada contribution i996107,

References

Allison, I., The mass budget of the Lambert Glacier drainage basin, Antarctica, *J. Glaciol.*, *22*, 223-235, 1979.

Allison, I., N. W. Young, and-i'. Medhurst, On reassessment of the mass balance of the Lambert Glacier drainage basin, Antarctica, *J. Glaciol.*, *31*, 378-381, 198S.

Barnett, "i'. I)., Recent changes in sea level and their possible causes, *C/ire Change*, *S*, 15-38, 1983.

Bentley, C. R., Evaluation of the mass balance of the Antarctic ice sheet: Plans for a coordinated international program, paper presented at the Joint NASA/NSF Sea-level Workshop, NASA, Miami, Fla., Nov. 15-1'?, 1995.

Bentley, C. R., and M. B. Giovinetto, Mass balance of Antarctica and sea level change, in *Proceedings of the International Conference on the Role of the Polar Regions in Global Change, 1990*, edited by G. Weller, C. L. Wilson, and B. A. B. Severin, pp. 481-488, Univ. of Alaska, Fairbanks, 1991.

Bindschadler, R., 1'.1.. Vornberger, and S. Shabtaie, The detailed net mass balance of the ice plain on Ice Stream B, Antarctica: A geographic information system approach, *J. Glac.*, *39*, 471-481, 1993.

Bloxham, J., D. Gubbins, and A. Jackson, Geomagnetic secular variation, *Philos. Trans. R.* Sot, *London, Ser. A*, .?29, 415-502, 1989.

Cazenave, A., I'. Gegout, G. Ferhat, and R. Biancale, Temporal variations of the gravity field from LAGEOS 1 and 1 AGEOS 2 observations, in *Global Gravity Field and Its Temporal Variations*, edited by R. }1. Rapp, A. Cazenave, and R. S. Nerem, pp. 141-1 S1, Springer-Verlag, New York, 1996.

(ho, B. F., Anthropogenic impact on global geodynamics due to reservoir water impoundment, *Geophys. Res. Lett.*, 22, 3s29-3s32, 1 99s.

Chao, B. F., and W. J', O'Connor, Effect of a uniform sca level change on the Earth's rotation and gravitational field, *Geophys. J.*, *93*, 191-193, 1 988a.

Chao, B. F., and W. 1'. O'Connor, Global surface-water-induced seasonal variations in the Earth's rotation and gravitational field, *Geophys. J.*, *94*, 263-270, 1988b.

Chao, B. 1", w. P. O 'Connor, A, T. C. Chang, D. K. Hall, and J. L. Foster, Snow load effect on the Earth's rotation and gravitational field, 1979 -198S, *J. Geophys. Res.*, 92, 9415-9422, 1987.

Cheng, M. K., R. J. Eanes, C. K. Shum, B. E. Schutz, and B. D. Tapley, Temporal variations in low degree zonal harmonics from Starlette orbit analysis, *Geophys. Res. Lett.*, *16*, 393-396, 1989.

Christensen, U. R., Heat transport by variable viscosity convection, 11, Pressure influence, non-Newtonian rheology and decaying heat sources, *Phys. Earth Planet. Inter.*, *37*, 183-205, I 985.

Conrad, C. l)., and B. H. Hager, The elastic response of tbc 1 Earth to interannual variations in Antarctic precipitation, *Geophys. Res. Lett.*, 22, 3183-3186, 1995.

dc Wolde, J. R., R. Bintanja, and J. Oerlemans, On thermal expansion over the last hundred years, *J. Clim.*, *8*, 2882-2891, 1995,

I Douglas, B. (', Global sca level rise, *J. Geophys. Res.*, 96, 6981-6992, 1991.

Douglas, B. C., Global sca level change: Determination and interpretation, *U.S.* Nell. *Rep. Int. Union Geod. Geophys. 1991-1994, 33, 1425-1432, 1995.*

Eanes, R. J., and S. V. Bettadpur, Temporal variability of Earth's gravitational field from satellite laser ranging, in *Global Gravity Field and Its Temporal Variations*, edited by R. 11. Rapp, C. Cazenave, and R. S. Nerem, pp. 30-41, Springer-Verlag, New York, 1996,

Fahnestock, M., R. Bindschadler, R. Kwok, and K. Jezek, Greenland ice sheet surface properties and ice dynamics from ERS-1SAR Imagery, *Science, 262, 1530-1534,* 1993.

Fang, M., B. t 1, Hager, and 'I'. A. Herring, Surface deformation caused by pressure changes in the fluid core, *Geophys. Res. Lett.*, *23*, 1493-1496, I 996.

Giovinetto, M, B., and (. R. Bentley, Surface balance in ice drainage systems of Antarctica, *Antarc. J. U. S., 20, 6-13,* 1985.

Hellmer, H. H., and S. S. Jacobs, Ocean interactions with the base of Amery Ice Shelf, Antarctica, *J. Geophys. Res.*, 97, 20,305-20,317, 1992,

Ivins, E. R., C. G. Sammis and (. F. Yoder, Deep mantle viscous structure with prior estimate and satellite constraint, *J. Geophys. Res., 98*, 4 S79-4 609, 1993.

Jacobs, S.S., and H. 11. Hellmer, Antarctic ice sheet melting in the Southeast Pacific, *Geophys. Res. Lett.*, 2.?, 957-960, 1996.

Jacobs, S. S., H. }1. Hellmer, C. S. M. Doake, A. Jenkins, and R. M. Frolich, Melting of icc shelves and the mass balance of Antarctica, *J. Glaciol., 38*, 375-387, 1992,

James, T. S., and E. R. Ivins, Present-day Antarctic ice mass changes and crustal motion, *Geophys. Res. Lett., 22,* 973-976, 199S.

Jenkins, A., and C. S. M. Doake, Icc-ocean interaction on Ronne Icc Shelf, Antarctica, *J. Geophys. Res., 96,* 791-813, 1991.

Krabill, W., R. Thomas, K. Jezek, K. Kuivinen, and S. Manizade, Greenland icc thickness changes measured by laser altimetry, *Geophys. Res. Lett., 22*, 2341-2344, 1995.

Lambeck, K., *The Earth's Variable Rotation*, 449 pp., Cambridge Univ. Press, New York, 1980.

Lambeck, K., and A. Cazenave, Long term variation in the length of day and climatic than.gc, *Geophys. J. R. Astron. Soc., 46, 555-573, 1976.*

Lucchita, B. K., C. E. Rosanova, and K. F. Mullins, Velocities of Pine Island Glacier, West Antarctica, from ERS-1SAR images, *Ann. Glaciol., 21*, 277-283, 1995.

Marlin, (". F., and D. P. Rubincam, Effects of Earth albedo on the LAGEOS 1 satellite, *J. Geophys. Res.,* 10/, 3215-3226, 1996.

McIntyre, N. F., A reassessment of the mass balance of the Lambert Glacier drainage basin, Antarctica, *J. Glaciol., .?1,* 34-38, 1985a.

McIntyre, N. 1'., Reply to "On reassessment of the mass balance of the Lambert Glacier drainage basin, Antarctica", *J. Glaciol., 31*, 381-382, 1985b.

Meier, M. F., ('contribution of small glaciers to global sea level, *Science, 226*, 1418-1421, 1984.

Meier, M. F., Role of land ice in present and future sea level change, in *Sea-Level Change*, pp. 171-184, Nat. Acad. Press, Washington, D.C., 1990.

Meier, M. F., Icc, climate, and sea level; Do we know what is happening?, in *Ice in the Climate System*, edited try W. R. Peltier, pp. 141-160, Springer-Verlag, New York, 1993.

Mitrovica, J. X., and W. R. Peltier, Pleistocene deglaciation and the global gravity field, .1, *Geophys. Res.,* 94, 13,651-13,671, 1989.

Mitrovica, J. X., and W. R. Peltier, A complete formalism for the inversion of postglacial rebound data: Resolving power analysis, *Geophys. J. Int., 104,* 267-288, 1991.

Mitrovica, J. X., and W. R. Peltier, Present-day secular variations in the renal harmonics of Earth's geopotential, *J. Geophys. Res., 98*, 4509 -4S26, 1993.

Munk, W. and R. Revelle, On the geophysical interpretation of the irregularit ics in the rotation of the Earth, *Mon.* Not. *R. Astron. Sm.,* 6, 331-343, 19S2.

Nerem, R. S., and S. M. Klosko, Secular variations of the zonal harmonics and polar motion as geophysical constraints, in *Global Gravity Field and Its Temporal Variations*, pp. 152-163, edited by R. H. Rapp, A. Cazenave, and R. S. Nerem,

pp, 1 52-163, Springer-Verlag, 1996.

O'Connell, R. J., Pleistocene deglaciation and the viscosity of the lower mantle, *Geophys. J. R. Astron.* Sot., *23*, 299-327, 1971.

Pari, G., and w. R. Peltier, The heat flow constraint on mantle tomography-based convection models: Toward a geodynamically self-consistent inference of mantle viscosity, J. *Geophys. Res., 100, 12,731-12,751, 1995.*

Peltier, W. R., Constraint on deep mantle viscosity from 1 AGEOS acceleration data, *Nature, 304*, 434-436, 1983.

Peltier, W. R., The Lageos constraint on deep mantle viscosity: Results from a new normal mode method for the inversion of viscoelastic relaxation spectra, *J. Geophys. Res.*, 90, 9411-9421, 1985.

Peltier, W. R., Global sca level and Earth rotation, *Science*, 240, 895-901, 1988.

Peltier, W. R., Ice age paleotopography, *Science*, 265, 195-201, 1994.

Peltier, W. R., and X. Jiang, Glacial isostatic adjustment and Earth rotation: Refined constraints on the viscosity of the mantle, *J. Geophys. Res., 101,* 3269-3290, 1996.

Peltier, W. R., and A. M. Tushingham, Global sca level rise and the greenhouse effect: Might they be connected?, *Science*, 244, 806-8 10, 1989.

Radok, U., R. G. Barry, D. Jenssen, R. A. Keen, G. N. Kiladis, B. McInnes, Climatic and physical characteristics of the Greenland icc sheet, report, Univ. of Colorado, Boulder, 1982.

Radok, U., T. J. Brown, D. Jenssen, I. N. Smith, and W. F. Budd, On the surging potential of polar icc streams, IV, Antarctic ice accumulation basins and their main discharge regions, Rep. DE/ER/601 97-5, Univ. of Colorado, Boulder, 1986.

Rubincam, D. P., Postglacial rebound observed by LAGEOS and the effective viscosity of the lower mantle, *J. Geophys. Res.*, 89, 1077-1087, 1984.

Sabadini, R., D. A. Yuen, and P. Gasperini, Mantle rheology and satellite signatures from present day glacial forcings, *J. Geophys. Res., 93*, 437-447, 1988.

Tackley, P. J., Effects of strongly variable viscosity on three-dimensional compressible convection in planetary mantles, J. *Geophys. Res., 101, 3311-3332,* 1996.

Thomas, R. 11. and C. R. Bentley, A model for Holocene retreat of the West Antarctic Icc Sheet, *Quat. Res., 10*, 150-170, 1978.

Trupin, A., and J. Wahr, Spectroscopic analysis of global tide gauge sca level data, *Geophys. J. Int., 100*, 441-453, J 990.

Trupin, A. S., Effects of polar ice on tbc Earth's rotation and gravitational potential, *Geophys. J. Int., 113*, 273-283, 1993.

'1 rupin, A, S., M. F. Meier, and J. M. Wahr, Effect of melting glaciers on the Earth's rotation and gravitational field: 196S-1984, *Geophys. J. Int., 108*, 1-15, 1992.

Trupin, A. S., D. A. Easson, and D. Han, Vertical motion and icc thickness variation in western North America, *Geophys. Res. lotf.*, 2.?, 253-256, 1996.

Tushingham, A. M., and W. R. Peltier, Ice-3G: A new global model of late Pleistocene deglaciation based upon geophysical predictions of postglacial relative sca level, *J. Geophys. Res., 96*, 4497-4523, 1991.

Vaughan, D. G., and C. S. M. Doake, Recent atmospheric warming and retreat of ice shelves on the Antarctic Peninsula, *Nature*, 379, 328-331, 1996.

Vermeersen, L. L. A., R. Sabadini, G. Spada, and N. J. Vlaar, Mountain building and Earth rotation, *Geophys. J. Int.*, *117*, 610-624, 1994.

Vondrak, J., C. Ron, I. Pesek, and A. Cepek, New global solution of Earth orientation parameters from optical astronomy in 1900-1990, *Astron. Astrophys.*, 297, 899-906, 1995.

Wagner, C. A., and D. C. McAdoo, Time variations in the Earth's gravity field detectable with geopotential research mission intersatellite tracking, *J. Geophys. Res.*, 91, 8373-8386, 1986.

Wahr, J., D. Han, A. Trupin, and V. Lindqvist, Secular changes in rotation and gravity: Evidence of postglacial rebound or of changes in polar ice?, *Adv. Space Res.*, *13(11)*, 257-269, 1993.

Wahr, J., D. Han, and A. Trupin, Predictions of vertical uplift caused by changing polar ice volumes on a viscoelastic Earth, *Geophys. Res. Lett.*, 22, 977-980, 1995.

Warrick, R., and J. Oerlemans, Sea level rise, in *Climate Change: The IPCC Scientific Assessment*, edited by J. T. Houghton, G. J Jenkins, and J. J. Ephraums, pp. 260-280, Cambridge Univ. Press, New York, 1990.

Warrick, R., H. Oerlemans, J. Woodworth, M. Meier, and C Le Provost, Changes in Sea Level, in *Climate Change 1995: The Science of Climate Change*, edited by J. J. Houghton, L. G. Meira Filho, B. A. Callander, N. Harris, A. Kattenberg, K. Maskell, pp. 359-405, Cambridge Univ. Press, New York, 1996.

Wessel, P., and W. H. F. Smith, Free software helps map and display data, *Eos Trans. AGU*, 72,441, 1991.

Wu, P., and W. R. Peltier, Glacial isostatic adjustment and the free air gravity anomaly as a constraint on deep mantle viscosity, *Geophys. J. R. Astron. Soc.*, 74, 377-449, 1983.

Yoder, C. F., J. G. Williams, J. O. Dickey, B. E. Schutz, R. J. Eanes, and B. D. Tapley, Secular variation of Earth's gravitational harmonic J_2 coefficient from LAGEOS and nontidal acceleration of Earth rotation, *Nature*, *303*, 757-762, 1983.

Yuen, D. A., and R. Sabadini, Viscosity stratification of the lower mantle as inferred by the J_2 observation, *Ann. Geophys.*, *3*, 647-654, 1985.

Yuen, D. A., R. C. A. Sabadini, J. Gasperini, and E. Boschi, On transient rheology and glacial isostasy, *J. Geophys. Res.*, *91*, 11,420 -11,435, 1986.

E. R. Ivins, Jet Propulsion laboratory, California Institute of Technology, 4800 Oak Grove Drive, MS 183-501, Pasadena, CA, 91109-8099.

T. S. James, Pacific Geoscience Centre, Geological Survey of Canada, 9860 W. Saanich Road, Sidney, British Columbia, Canada V8L 4B2. (e-mail james@pgc.emr.ca)

(Received April 22, 1996; revised August 21, 1996; accepted September 18, 1996.)

Paper Number 96JB02855.

0148-0227/97/96JB-02855$09.00

JAMES AND IVINS: ANTARCTIC GLOBAL GEODETIC SIGNATURES

Figure Captions

Figure 1. Map of Antarctic surface elevation and drainage systems. Contour interval is 0.5 km. Boundaries of major drainage systems (ice divides) are marked with capital letters at the coast; interior ice divide intersections are marked with lower case letters [after *Giovinetto and Bentley*, 1985].

Figure 2. Plan view and cross section of ice sheet grounded below sea level [after *Thomas and Bentley*, 1978].

Figure 3. Map of surface mass imbalance rates (in 100 kg/m^2 per year). The inland ice systems for which a net imbalance determination could be made are delineated with heavy lines and are numbered according to Table 1. Primed and double-primed letters indicate subdivisions of the major drainage basins, Circles mean no significant imbalance, pluses mean significant positive net imbalance. Figure is after *Bentley and Giovinetto [1991]*.

Figure 4. Same as Figure 3, but for combined inland and ice shelf systems for which a net imbalance determination could be made. These regions are identified with bracketed numbers according to Table 2. Also shown for each region is the basal ice shelf melt rate (meters per year) required for steady state. Circles mean no significant imbalance, plus and minus mean significant positive and negative net imbalance, respectively. Figure is after *Bentley and Giovinetto [1991]*.

Figure 5. Same as Figure 3, but for systems without net mass imbalance determinations. These systems, delineated with thick lines, are located along the coast. Figure is after *Bentley and Giovinetto [1991]*.

Figure 6. Four scenarios of present day Antarctic ice sheet mass change, three derived from Bentley *and Giovinetto [1991]*, (a) scenario 1, (b) scenario 2 by mass, (c) scenario 2 by area, and one from *Jacobs et al. [1992]*, (d) J92 scenario. Imbalance is represented in millimeters per year of ice thickness change.

Figure 7. The (a) T0 [after *Trupin*, 1993] and (b) NE Greenland scenarios. Ice height change is shown in Figure 7a in millimeters per year and in figure 7b in meters per year.

Figure *8,* The observed polar motion direction and magnitude and the directions and magnitudes resulting from the present day scenarios of ice mass change in a (top) southern and (bottom) northern hemisphere perspective. Ohs is observed [*Vondrak et al.*, 1995]; *1*, scenario 1; 2a, scenario 2. by area; 2m, scenario 2 by mass; J92, J92 scenario; IC, mountain glaciers and small ice caps; T0, T0 scenario; and Gr, NE Greenland scenario. The polar motion magnitude for the T0 scenario (dotted line) is not shown to scale (see Table 4; the arrow should be 30°/0 larger). The observed polar wander is directed toward Hudson Bay. Apparently, postglacial rebound is capable of explaining most of this signature [see *Peltier and Jiang*, 1996].

Figure 9. (a) A tutorial example of large, positive, odd-degree zonal changes arising from Greenland ablating and Antarctica accumulating ice mass. (b) The weighting functions - $P_l(\cos\theta)$ for degrees 2 through 8 required to derive zonal harmonic coefficients J_l from a given surface load $\sigma(\theta,\lambda)$ (equation (5)). Positive values of the weighting functions are shaded. Numbers on the periphery indicate the corresponding spherical harmonic degree.

Figure 10. The $\dot{J}_l$ predictions for the four Antarctic scenarios developed in this study (circles) for degrees 2 through 7. On the abscissas are ξ_A, the Antarctic contribution to sea level change, and on the ordinates are the $\dot{J}_l$ predictions. Also shown above each frame are the parameters of the best fitting straight line drawn through the 4 circles (J2dot = $\dot{J}_2$, etc., and sldot = ξ), drawn as a solid line. Also shown are the $\dot{J}_l$ values obtained by *Trupin [1993]* for his steady-state (crosses, long-dashed line), thinning interior (triangles, dotted line), and thickening interior (pluses, short-dashed line) scenarios.

Figure 11. $\dot{J}_l$ predictions for the Greenland ice sheet for *Trupin*'s *[1993]* outer Benson line (OB) (triangles, short-dashed line) and inner Benson line (IB) (pluses, long-dashed line) scenarios as a function of Greenland contribution to sea level change ξ_G for degrees 2 through 7. The solid line is the sea level/$\dot{J}_l$ dependence obtained by scaling the NE Greenland scenario $\dot{J}_l$ prediction by the Greenland contribution to sea level change. The linear dependences for the three scenarios are given in each frame. The Greenland sea *level*/$\dot{J}_l$ dependence used in the following global composite analysis is given above each frame and is the average of the sea level/$\dot{J}_l$ slopes found for *Trupin*'s *[1993]* two scenarios, " "

Figure 12. Postglacial rebound $\dot{J}_l$ predictions. Degrees 2 through 5 are given and the ICE-3G [*Tushingham and Peltier, 1991*] ice load history is assumed. The homogeneous lower mantle (HLM) case (solid lines) refers to *Mitrovica and Peltier*'s *[1993]* calculations, in which the whole lower mantle viscosity is varied. The 650-km boundary layer (650BL) case (dashed lines) refers to *Ivins et al.*'s *[1993]* calculations, in which the lower mantle viscosity is varied, except for a 650-km-thick boundary layer at the core-mantle boundary (2235.5 to 2885.5 km depth). The boundary layer has a fixed high viscosity of 6 x 10^{23} Pa s. The horizontal lines in the degree 2 frame show the observed $\dot{J}_2$ and associated uncertainty, as reported by *Nerem and Klosko [1996]*.

Figure 13. Contoured normalized standard deviation d (see text for definition) for global composite scenarios assuming the HLM glacial rebound $\dot{J}_l$ values (Figure 12, **solid** line) and other source parameters as described in the text under baseline assumptions. The contours indicate the level of agreement (smaller values equal better agreement) between predicted and observed $\dot{J}_l$ values as lower mantle viscosity and the Antarctic contribution to sea level change are varied for total sea level change rate $\dot{\xi}$ ranging from 0 to 2.5 mm/yr. Global composite scenarios A through D, as described in Tables 6 and 7, are marked accordingly. Subordinate tick marks on the horizontal axis are located at factors of 2 and 5 times the labeled values. Contours are drawn at standard deviation values of 1, 2, 3, 5, 10, 20, 30...

Figure 14. Same as Figure 13, except the 650-km boundary layer (650BL) postglacial rebound case is assumed (Figure 12, dashed line). The abscissas refer to the lower mantle viscosity above the boundary layer. See Tables 6 and 7 for the details of global composite scenarios E through J.

Figure 15. A summary of the minimum standard deviation as different source assumptions and observed $\dot{J}_l$ values are varied. (left) Paths (arrows) taken by the minimum standard deviation as total sea level is varied, with the differing symbols indicating assumed total sea level rise and the differing line types indicating different assumptions or observed $\dot{J}_l$ values. The paths are drawn relative to lower mantle viscosity (horizontal axis) and Antarctic contribution to sea level (vertical axis), similar to Figures 13 and 14. (right) Actual corresponding standard deviation values. The standard curves (solid line) in Figures 15a-15f come from Figure 13 (*Nerem and Klosko [1996]* $\dot{J}_l$ observations and the ICE-3G postglacial rebound calculations). (a) $\dot{J}_l$ observations changed to *Cazenave et al.*'s [1996] and *Cheng et al.*'s [1989] values (see Table 8), and (b) their standard deviations. (c) The thermal expansion effect on sea level rise is doubled and the mountain glacier and small ice caps' contribution to sea level rise and $\dot{J}_l$ doubled, and (d) their standard deviations. (c) Antarctic sea *level/*$\dot{J}_l$ parameterization changed to *Trupin*'s [1993] steady-state model (see long-dashed lines of Figure 10) and *Fang et al.*'s *[1996]* estimate of the J_2 contribution from pressure effects at the core-mantle boundary (CMB) is included, and (f) their standard deviations.

Figure 16. Same as Figure 13, but with no constraint from $\dot{J}_3$. *Eanes and Bettadpur*'s [1996] J_2 and J_4 values are used (Table 8).

Table 1. Net Mass Imbalance $\dot{M}$ and Equivalent Ice Height Change $\dot{\eta}$ **for** Inland **Ice** Systems

	[*Bentley and Giovinetto, 1991*]		This Study	
System	$\dot{M}$ Gt/yr	Significant imbalance?	Area (10^3 km^2)	$\dot{\eta}$
1. Jutulstraumen*	5	no	150	36
2. Eastern Queen Maud Land	0	no	*450*	0
3. Eastern Enderby Land	3	no	100	33
4. Lambert Glacier (Allison/McIntyre)†	3917	yes/no	800	53/10
5, Western Wilkes Land (Combined)	4	no	850	5
6. East Antarctica onto Ross Ice Shelf	26	yes	1800	16
7. West Antarctica onto Ross Ice Shelf	-8	no	600	-14
8. Thwaites Glacier	5	no	250	22
9. Pine island Glacier	50	yes	2s0	218
10. Rutford Ice Stream	-6	no	50	-130
Totals	118.5		5300	

*See Figure 3 for numbered regions,
†[*Allison, 1979; Allison et al.,* 1985; *McIntyre,* 1985a, b]

Table 2. Net Mass Imbalance $\dot{M}$ and implied Steady State Basal Melt Rate for Combined Inland Ice and Ice Shelf System

System	*Bentley and Giovinetto [1991]* $\dot{M}$ (Gt/yr)	Basal Melt Rate (m/yr)	Reasonable?
11. Amery Ice Shelf* (Allison/McIntyre)†	83/51	1.5/0.9	no
12. George VI Ice Shelf	48	2.1	yes
13. Western Ronne Ice Shelf	44	0.37	yes
14. Eastern Ronne Ice Shelf	79	0.28	no
15. Filchner Ice Shelf	47	0.35	yes
16. Brunt & Riiser-Larsen Ice Shelves	-37	0.16	no

* See Figure 4 for numbered regions.
† [*Allison, 1979; Allison et al., 1985; McIntyre*, 1985a, b]

Table 3. Icc Shelf Melting Rates From *Jacobs et al.* [1992] (J92) and Amount of Mass Removed From Scenario 2 by Area to Obtain the J92 Scenario

Ice Shelf System	Net Melt Rate From J92		Mass Removal to Obtain J92 Scenario	
	Gigatons per Year	Percent of Total	Gigatons pet Year	Percent of Total
Filchner-Ronne	202	38	21?	47
Ross	79	15	68	15
George VI	49	9	43	10
Amery	23	4	36	8
Within 100 km of Ice Fronts	173	33	91"	20
Total	526		450	

● }lcrc59Cit/yl are from Enderby Land and 32 Gt/yr are from other narrow shelves

'1'able 4. Rates of Sea Level Rise $\dot{\xi}$, Ice Sheet Mass Change $\dot{M}$, and Secular Polar Motion $\dot{\mathbf{m}}$.

	Ice Sheet Scenario								
Global Rate Quantity	Scenario 1	Scenario 2 by Area	Scenario 2 by Mass	J92 Scenario	*Trupin* [1993]	This study	Mountain and Small Ice Caps*	Mountain Glaciers NE Greenland	Observed
$\dot{\xi}$, mm/yr	-0.11	*-0.8*	*-1.10*	0.44	0	0	0,38	0.91	1.51
$\dot{M}$, Gt/yr	39	290	400	-160	0	0	-138	-331	
$\lvert\dot{\mathbf{m}}\rvert$, mas/yr	0.48	*0.31*	0.56	1.13	4.23	4.46	0.36	2.43	3.3‡
γ_{NH}#	206	79	120	128	259	258	152	330	282
γ_{SH}	26	2.$9	300	308	79	78	332	150	102

J92 scenario is based on *Jacobs et al.* [1992]. The mas are milliseconds of arc.
*Data from *Meier* [1 984].
†Value is Intergovernmental Panel on Climate Change (IPCC) best estimate [*Warrick and Oerlemans*, 1990].
‡Value is from *Vondrak et* rd. [1 995].
#Direction y of secular polar motion $\dot{\mathbf{m}}$ given in °E of Greenwich in a northern (γ_{NH}) and southern (γ_{SH}) hemisphere perspective.

I'able S. Secular Zonal Gravitational Coefficient J_l Rates

	Ice Sheet Scenario							
						T0	Mountain Glaciers	
Degree 1	Scenario 1	Scenario 2 by Area	Scenario 2 by Mass	J92 Scenario	*Trupin* [1993]	This Study	and Small Ice Caps	NE Greenland
2	-4.6	-31.6	-41.4	17.8	9.s	9.6	8.7	*36.4*
3	5.2	32,6	40.2	-19.1	-20.8	-20.8	4.0	35.8
4	.5,4	-30.1	-33.5	18.7	34.2	34,1	0.7	*35.6*
5	S.6	27,4	26.7	-18.5	-47.4	-47.2	0.2	*28.2*
6	-5,2	-20.5	-14.6	16.2	58.6	58,3	-1,0	25.0
7	5.(I	15,7	6.2	-15.1	-66.8	-66.1	-1.0	17.0
8	-4.4	-9.3	3.5	13,3	70.9	69,9	-0,4	11.2

Rates arc in 10"12 yr^{-1}.

Table 6. Global **Composite** Scenario Definitions

Composite Scenario*	Sea **Level** Change, mm/yr			Lower Mantle Viscosity (Pas)	Standard Deviation
	Total	Antarctic	Greenland		
A	1.0	0.3	-0.08	2×10^{21}	1,48
B	1.5	0.7	0,02	5×10^{21}	1.69
C	1.5	0.4	0.32	5×10^{22}	0,86
D	2.0	0.8	0.42	2×10^{22}	0.92
E	1.0	0.2	0.02	5×10^{22}	0.66
F	1.5	0.5	0,22	5×10^{20}	0.58
G	1.5	0,6	0.12	1×10^{22}	1.18
H	2.0	0.9	0.32	1×10^{21}	1.70
I	2.0	1.0	0,22	5×10^{21}	0.73
J	2.5	1,3	0.42	2×10^{21}	0.19

*Scenarios A-D are homogeneous lower mantle (HLM) scenarios (Figure 13) and Scenarios E-J are 650-km boundary layer (650BL) scenarios (Figure 14).

I-Value refer to viscosity of the whole lower mantle for HLM scenarios and to viscosity of lower mantle above the high-viscosity boundary laycrfor'the 650BL scenarios.

'1'able 7. $\dot{J}_l$ Predictions and Residuals for Global Composite Scenarios

	$\dot{J}_l$ Values, by Degree, in 10^{12} /yr*											
	Observed $\dot{J}_2$. -27.7 ±2.5				observed $\dot{J}_{3l}$ = 15.7 ± 3.S				Observed $\dot{J}_4$ = 2.0 ± 14.6			
Scenario	A	G	PGR	Res	A	G	PGR	Res	A	G	PGR	Res
A (1.48)	11.8	-3.0	-40.8	-4.5	-21.1	-4.1	38.3	-1.52	11.5	-2,5	-33.7	26.0
B (1.69)	27.3	0.8	-61.1	-3.3	-46.9	1,0	61.0	-3.6	25.4	0.6	-59.8	35.1
C (0.86)	15.7	*12,0*	*-61.1*	*-2.9*	*-27.6*	*16,3*	*25,2*	*-2.4*	*15.0*	10.0	*-32,6*	9.0
D (0.92)	31,2	]5,7	-84.2	1.0	-53,3	21.4	38.5	5.0	28.9	13.0	-48.9	8.4
E (0.06)	7.9	0.8	-45,4	0.3	-14,7	1.0	24.0	1.2	8.0	0.6	-23.2	15.9
F (0.58)	19,6	8.2	-64.3	0.0	-34.0	11.2	31.0	3.3	18.5	6.8	-18.8	-5.1
(i (1.18)	23,4	4.5	-64.8	0.s	-40.5	6.1	50.4	-4,5	21.9	3.7	-47.3	23.0
H (1.70)	35.0	12.0	-90.1	6.7	-59.8	16.3	59.4	-4.5	32.3	9,9	-42.0	1.1
1 (0.73)	38.9	8.2	-83.4	-0.1	-66. I	11.2	66.2	0.3	35.8	6.8	-59.6	18.3
J (O. 19)	50.s	15.7	-102.1	-0.5	-85.5	21.4	76.3	-0.7	46.'2	13.0	-60.1	2.2

Values in parentheses arc standard deviations.

* A is Antarctica; G, Greenland; PGR, postglacial rebound; Res, Observed - $\sum$Predicted (predicted includes mountain glaciers and small ice caps, sec Table 5); observed values arc from *Nerem and Klosko* [1996] ($\dot{J}_{3l} = \dot{J}_3 + 0.837\dot{J}_5$). Scenarios A-D are ICE-3G scenarios (Figure 13); scenarios E-J are 650BI scenarios (Figure 14).

Table 8. $\dot{J}_l$ Satellite Solutions

Reference	$\dot{J}_2$	$\dot{J}_{31}$	$\dot{J}_3$	$\dot{J}_4$	Standard Deviation
Nerem and Klosko [1996]	-27.7 ± 2.5	15.7 ± 3.5		2 ± 14,6	6.9
Cazenave et al. [1996]	-30 ± 3		-17 ± 1	-8 ± 15	11.4
Cheng et al. [1989]	-25 ± 3		-1 ± 3	3 ± 6	4.8
Eanes and Bettadpur [1996]	-25.6 ± 3,4			-9 ± 13	5.3

Values in 10^{-12} yr^{-1}.

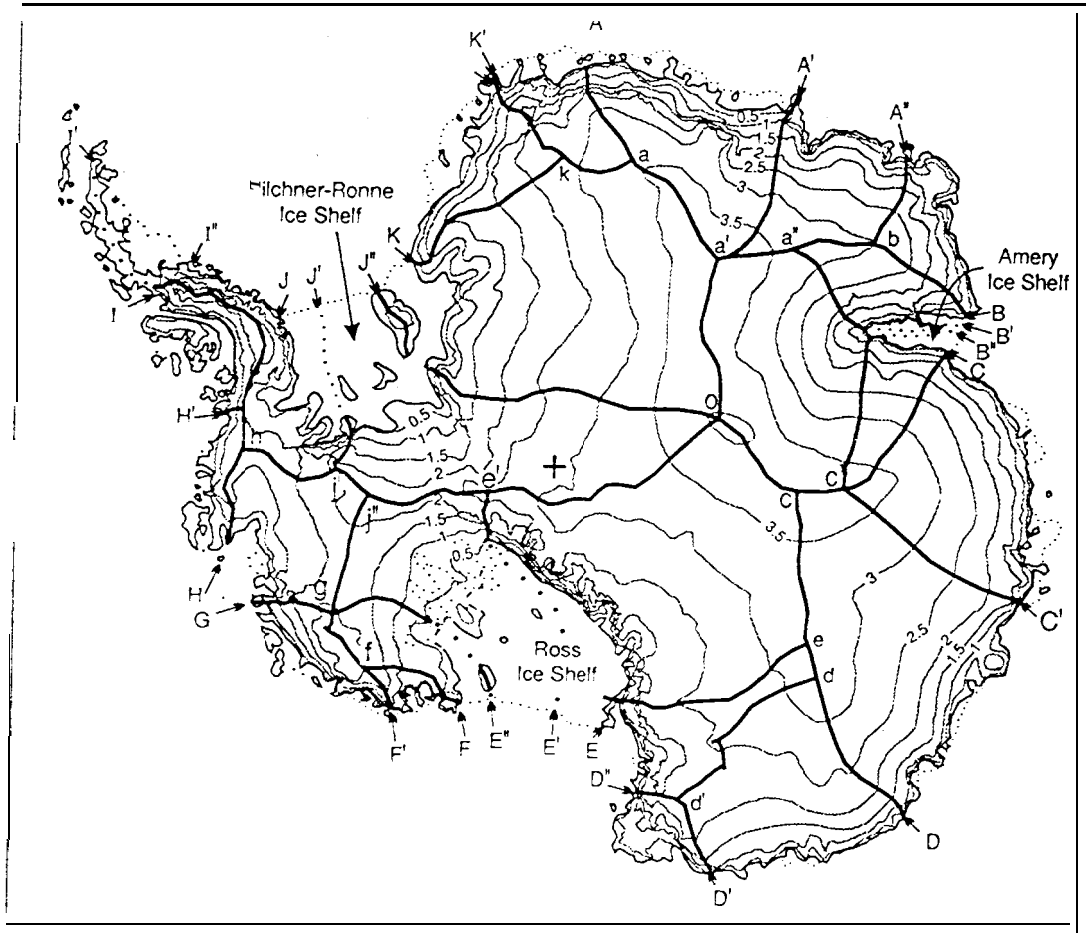

TJ940901.cdr

Figure 1.

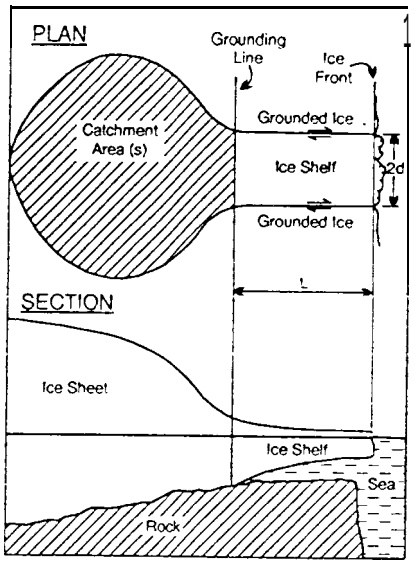
PLAN
Grounding Line
Ice Front
Grounded Ice
Catchment Area (s)
Ice Shelf
2d
Grounded Ice
L
SECTION
Ice Sheet
Ice Shelf
Sea
Rock

Figure 2.

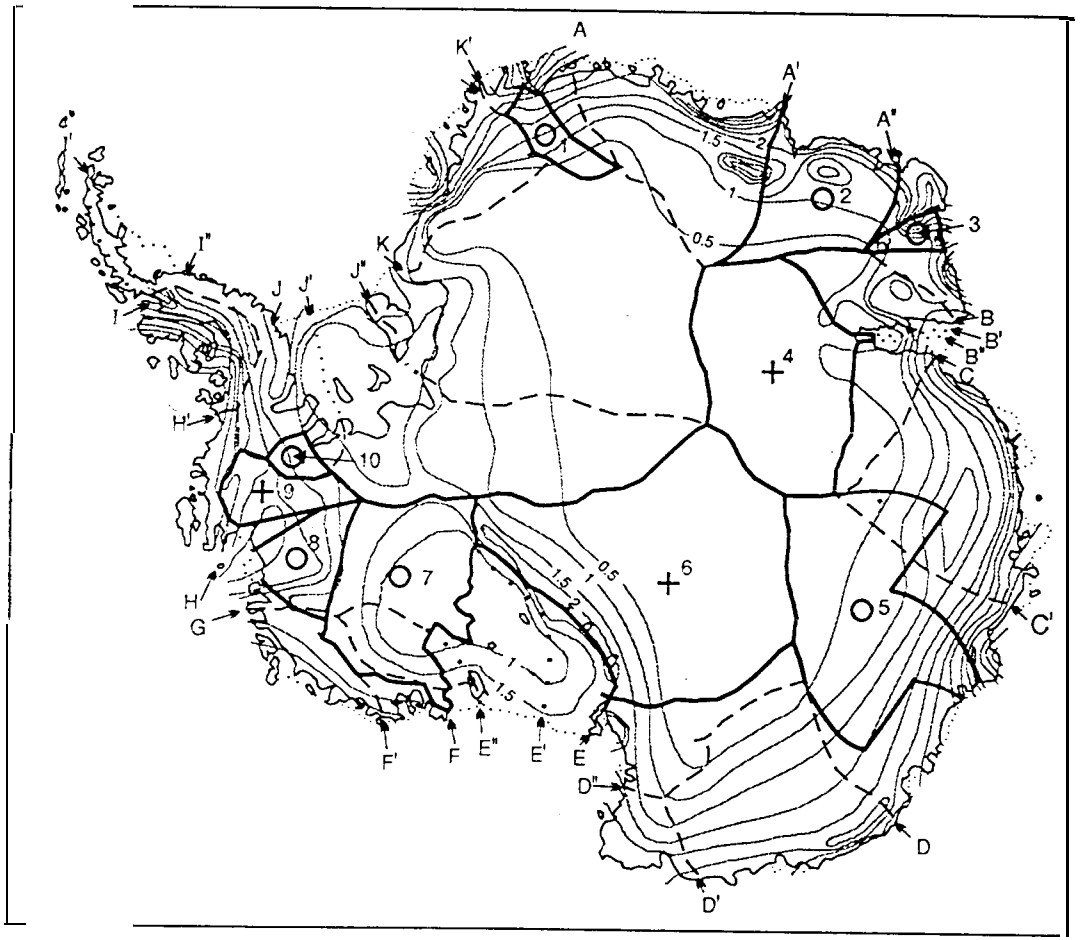

TJ94090A.cdr

Figure 3.

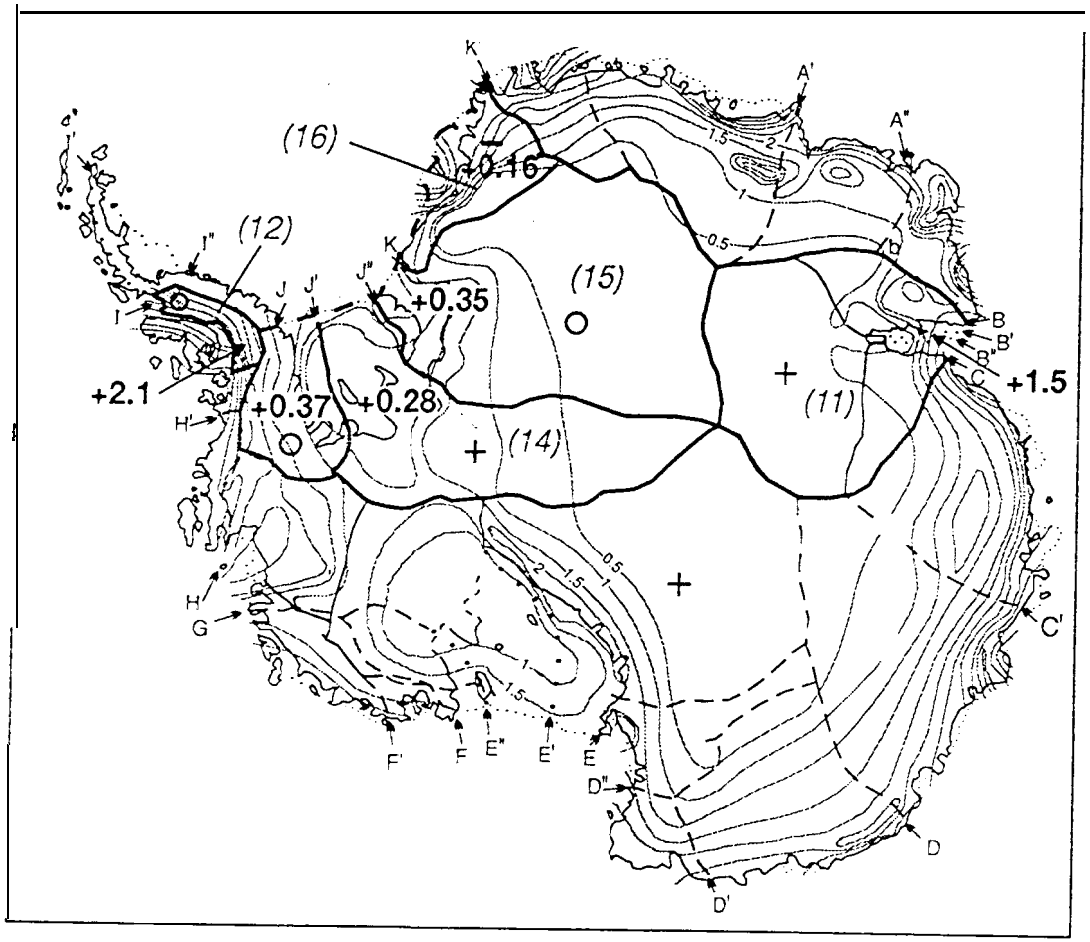

TJ94090B.cdr

Figure 4.

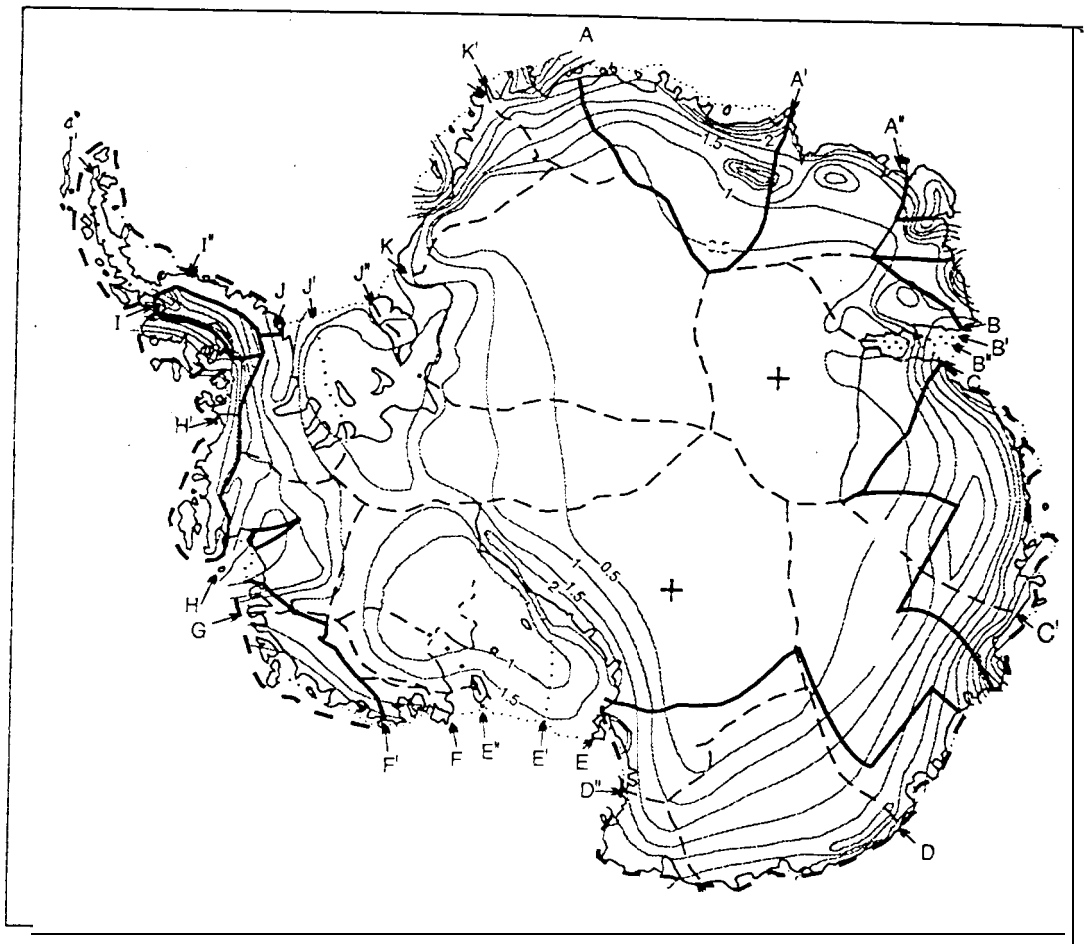

Figure 5.

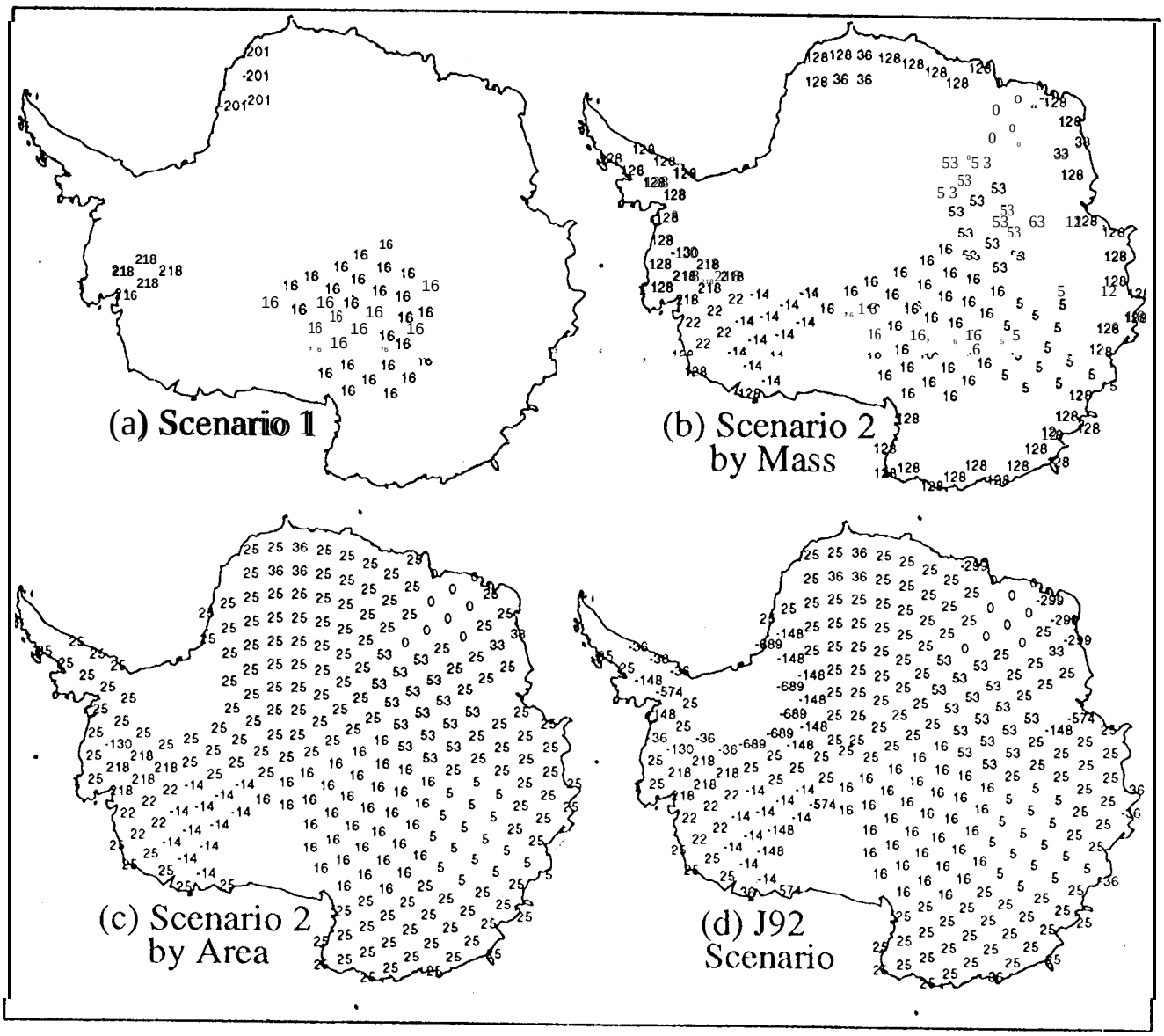
(a) Scenario 1
(b) Scenario 2 by Mass
(c) Scenario 2 by Area
(d) J92 Scenario

Figure 6.

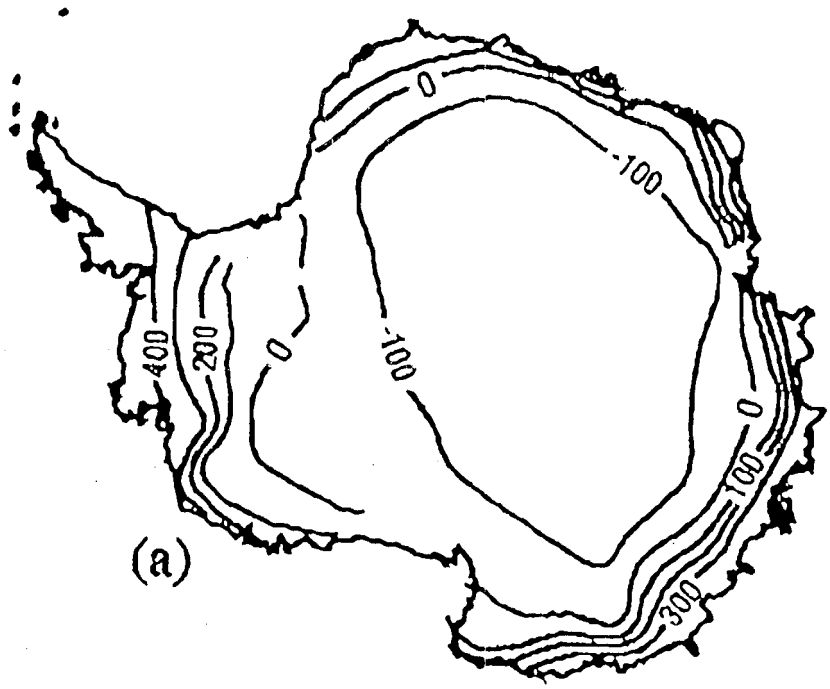
0
-100
400
200
0
-100
0
100
300
(a)

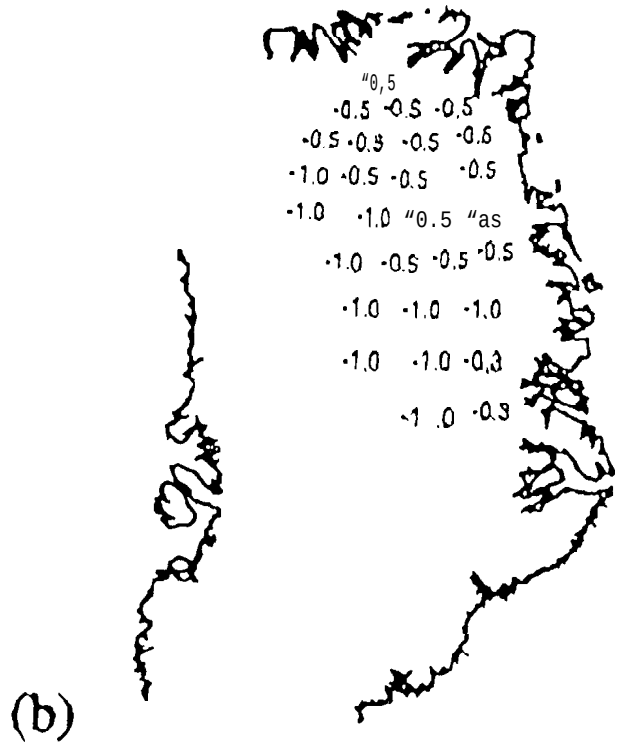
"0,5
-0.5 -0.5 -0.5
-0.5 -0.5 -0.5 -0.5
-1.0 -0.5 -0.5 -0.5
-1.0 -1.0 "0.5 "as
-1.0 -0.5 -0.5 -0.5
-1.0 -1.0 -1.0
-1.0 -1.0 -0.3
-1 .0 -0.3
(b)

Figure 7.

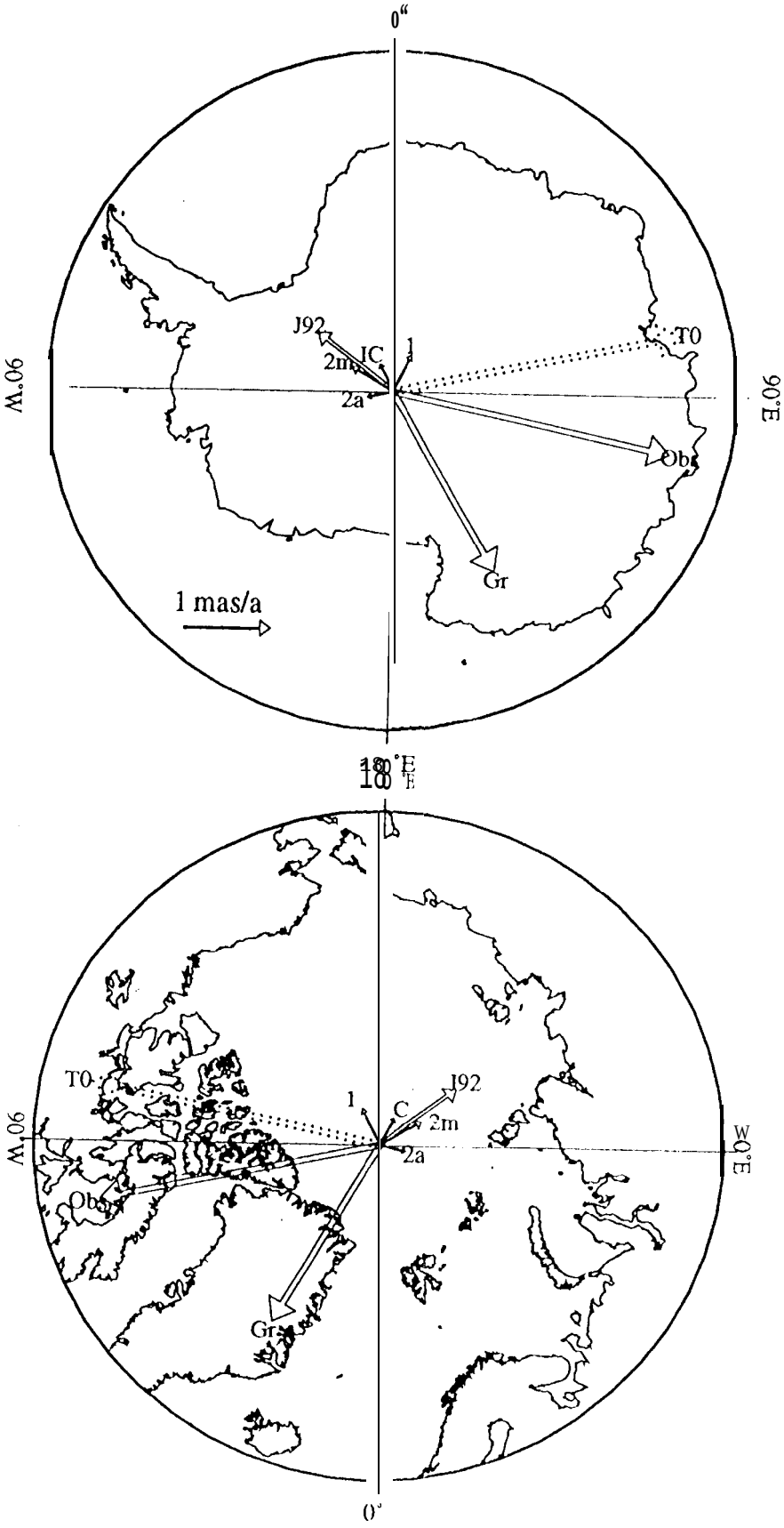
0°
90°W
90°E
J92
2m
IC
1
2a
T0
Obs
Gr
1 mas/a
180°E
T0
1
C
J92
2m
2a
90°W
0°E
Obs
Gr
0°

Figure 8.

Greenland retreats / Antarctica accumulates

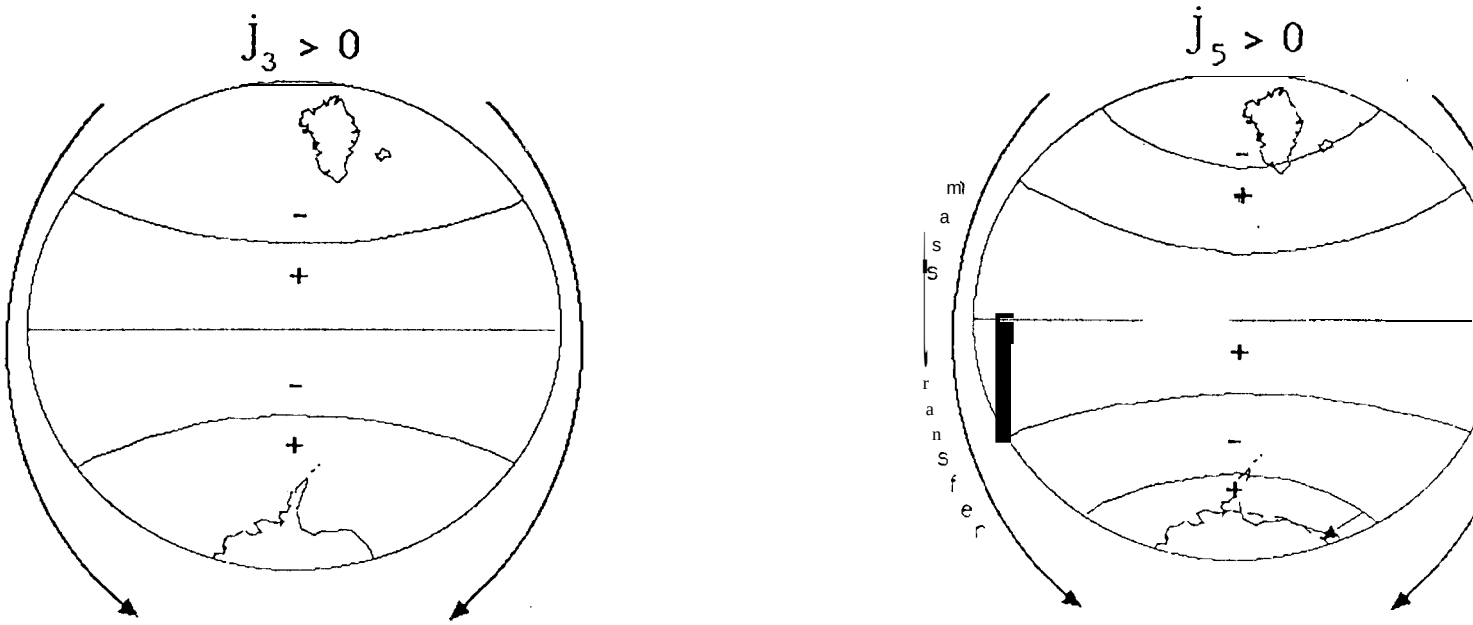

(a)

zonal latitudinal sensitivity

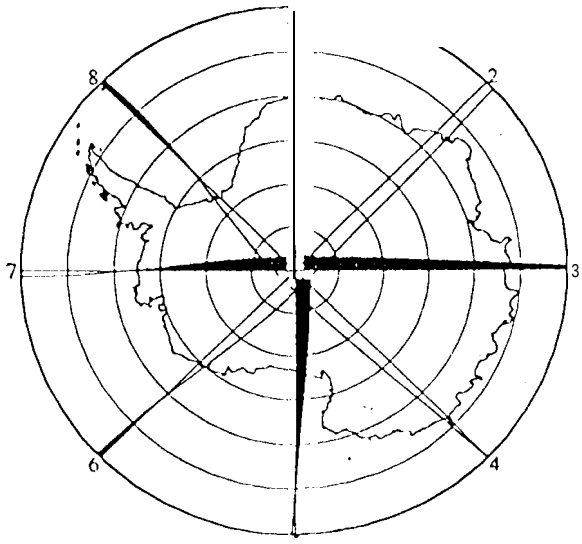

(b)

Figure 9.

Degree 2: J2dot = 38.7sldot + 0.2

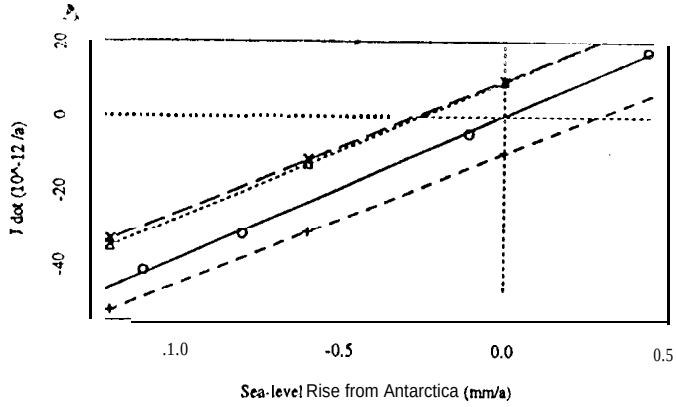

Degree 3: J3dot = -38.9sldot -0,5

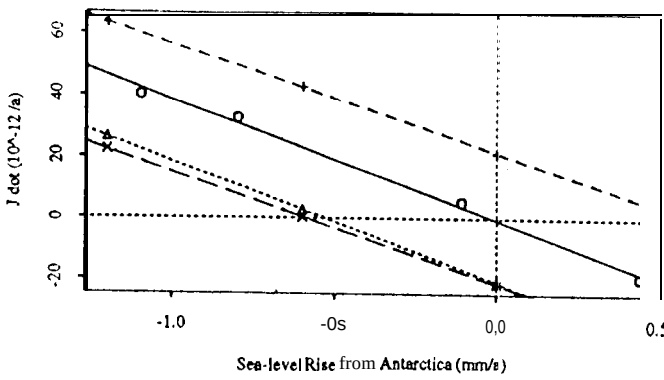

Degree *4:* J4dot = 34.7sldot + 1.1

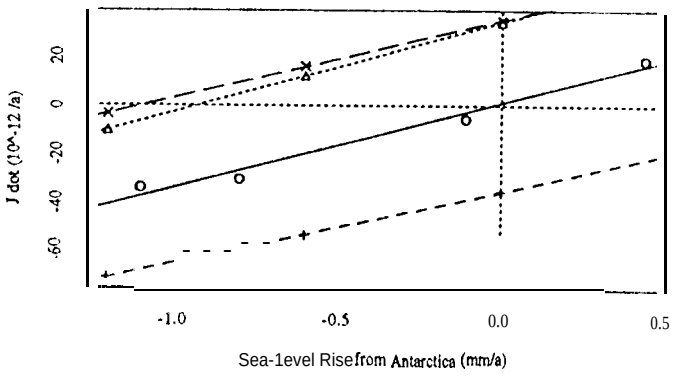

Degree *5:* J5dot = -30.4sldot -1.6

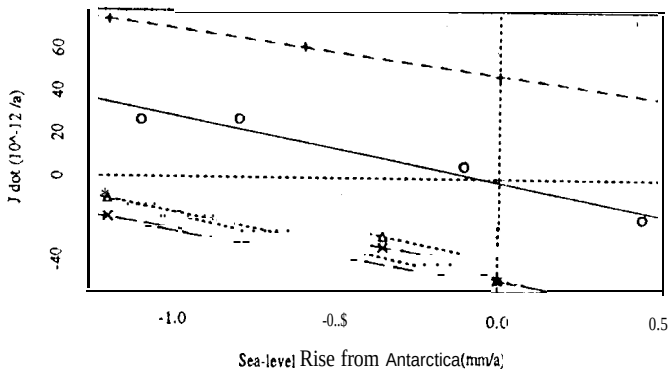

Degree 6: J6dot = 21 .3sldot + 2.3

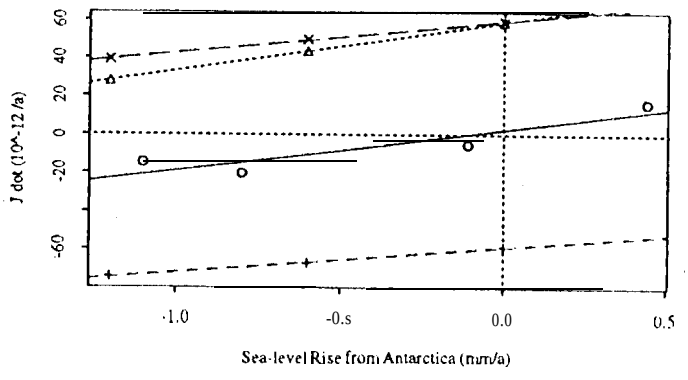

Degree 7: J7dot = -15.1sldot -2.9

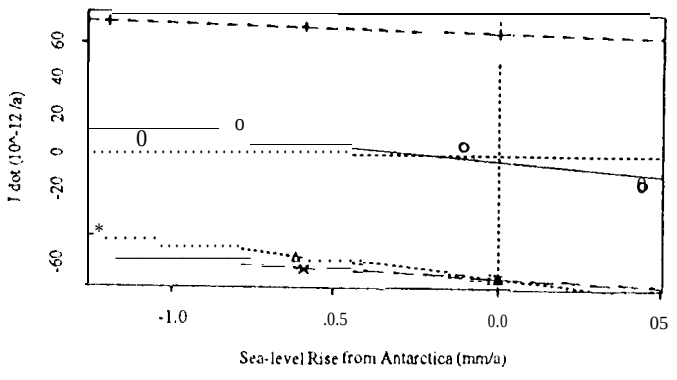

Figure 10.

Degree 2: J2dot = 37.4sldot

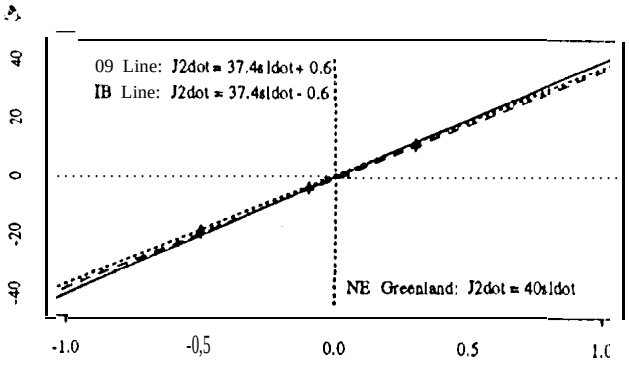

Sea-level Rise from Greenland (mm/a)

Degree 3: J3dot = 34.2sldot

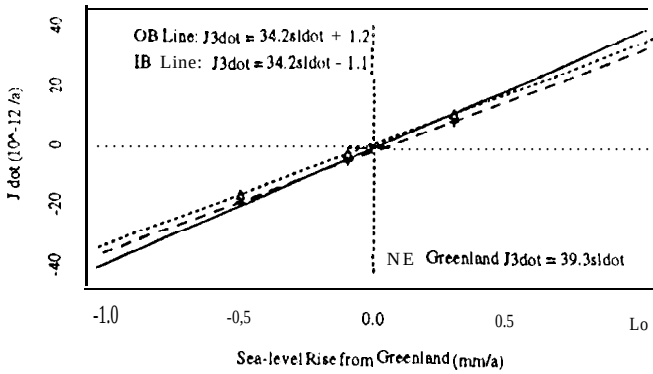

Sea-level Rise from Greenland (mm/a)

Degree 4: J4dot = 30.9sldot

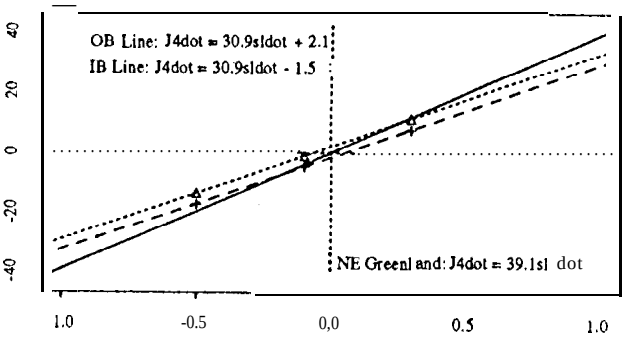

Sea-level Rise from Greenland (mm/a)

Degree 5: J5dot = 20,1 sldot

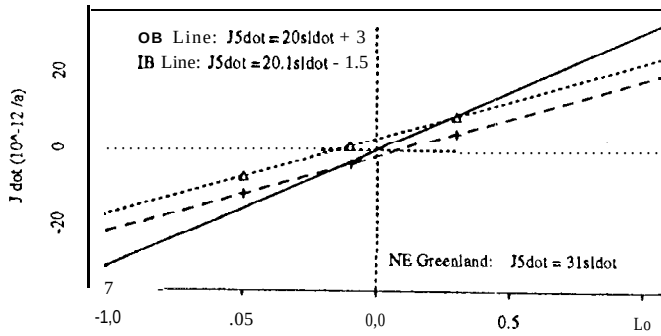

.%.-level Rise from Greenland (nun/a)

Degree 6: J6dot = 14.8sldot

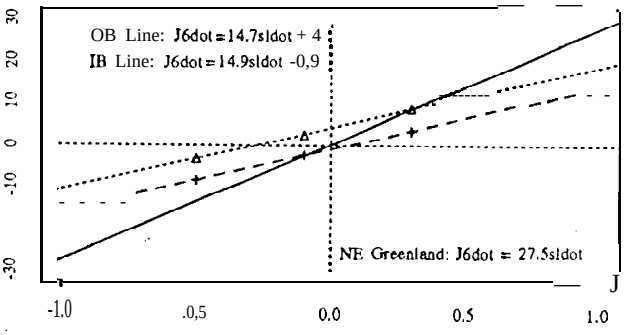

Sea-level Rise from Greenland (mm/a)

Degree 7: J7dot = 5.5sldot

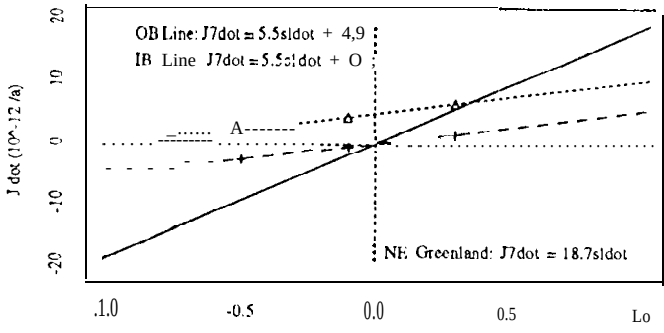

Sea-level Rise from Greenland (mm/a)

Figure 11.

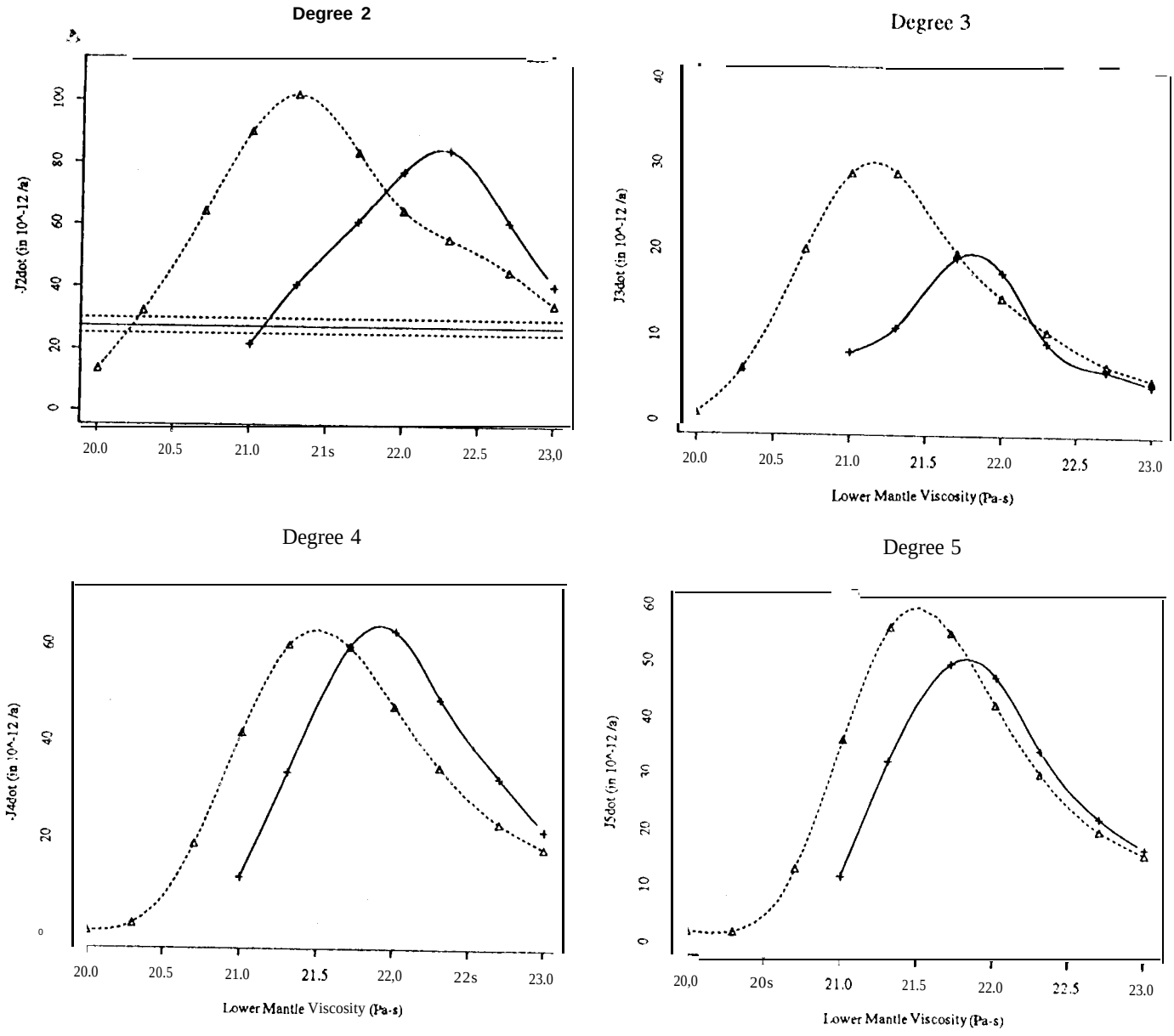
Degree 2
J2dot (in 10^-12 /a)
0
20
40
60
80
100
20.0
20.5
21.0
21s
22.0
22.5
23,0
Degree 3
J3dot (in 10^-12 /a)
0
10
20
30
40
20.0
20.5
21.0
21.5
22.0
22.5
23.0
Lower Mantle Viscosity (Pa-s)
Degree 4
J4dot (in 10^-12 /a)
0
20
40
60
20.0
20.5
21.0
21.5
22,0
22s
23.0
Lower Mantle Viscosity (Pa-s)
Degree 5
J5dot (in 10^-12 /a)
0
10
20
30
40
50
60
20,0
20s
21.0
21.5
22.0
22.5
23.0
Lower Mantle Viscosity (Pa-s)

Figure 12.

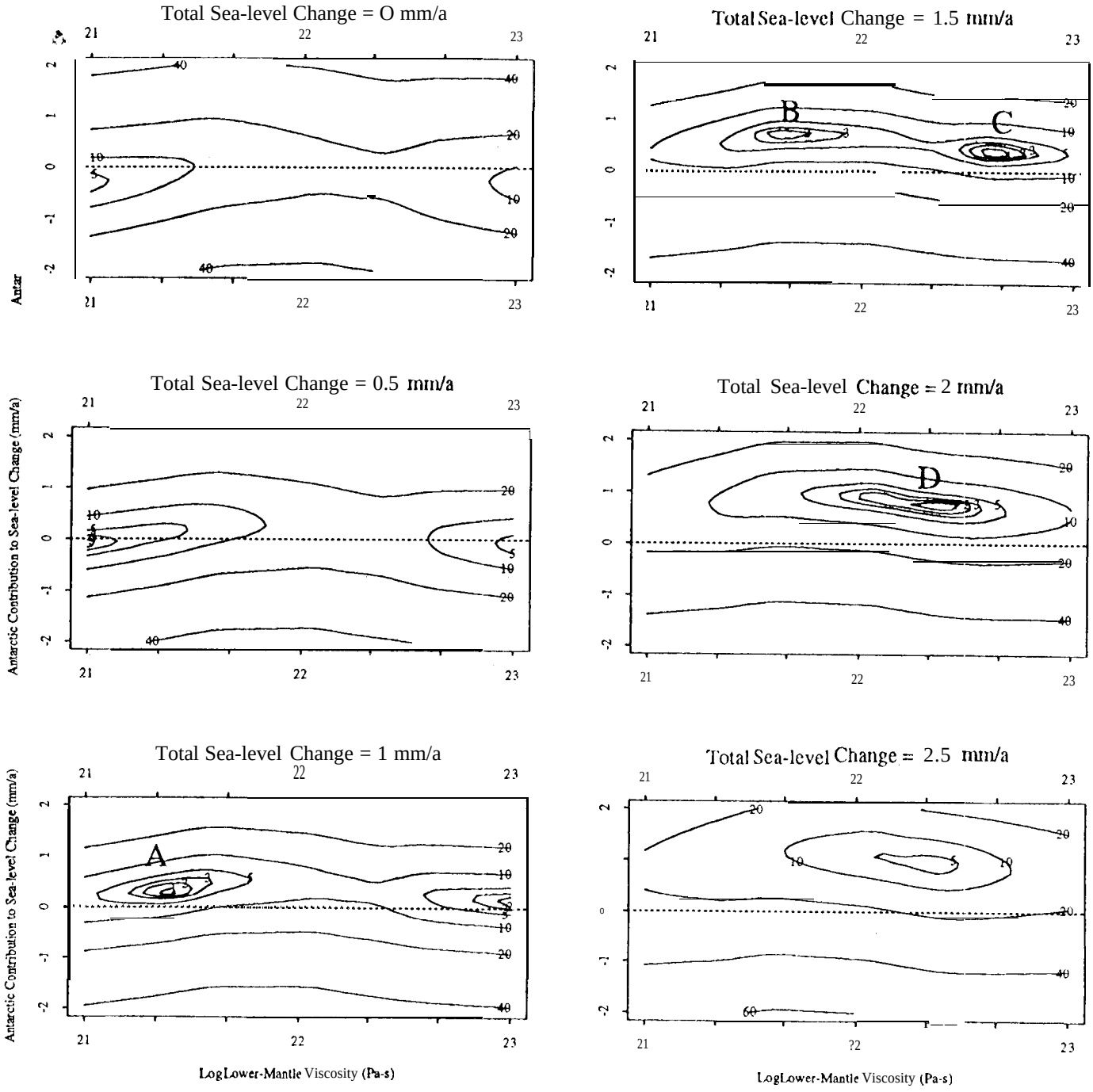
Total Sea-level Change = O mm/a
Total Sea-level Change = 1.5 mm/a
Total Sea-level Change = 0.5 mm/a
Total Sea-level Change = 2 mm/a
Total Sea-level Change = 1 mm/a
Total Sea-level Change = 2.5 mm/a
Antarctic Contribution to Sea-level Change (mm/a)
LogLower-Mantle Viscosity (Pa-s)
A
B
C
D

Figure 13.

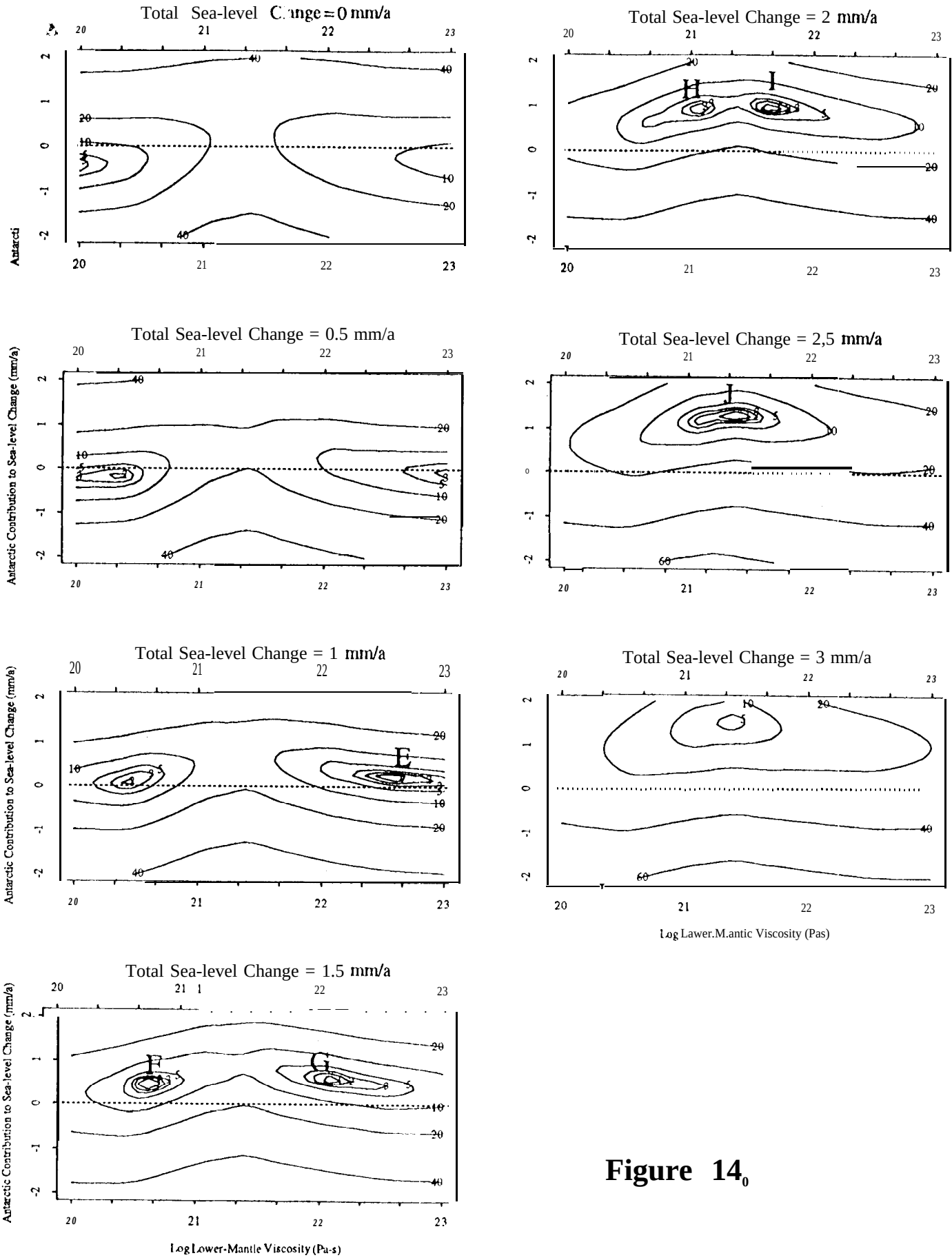
Total Sea-level Change = 0 mm/a
Total Sea-level Change = 2 mm/a
Total Sea-level Change = 0.5 mm/a
Total Sea-level Change = 2,5 mm/a
Total Sea-level Change = 1 mm/a
Total Sea-level Change = 3 mm/a
Total Sea-level Change = 1.5 mm/a
Antarctic Contribution to Sea-level Change (mm/a)
Log Lower-Mantle Viscosity (Pa-s)
Log Lawer.M.antic Viscosity (Pas)

Figure 14.

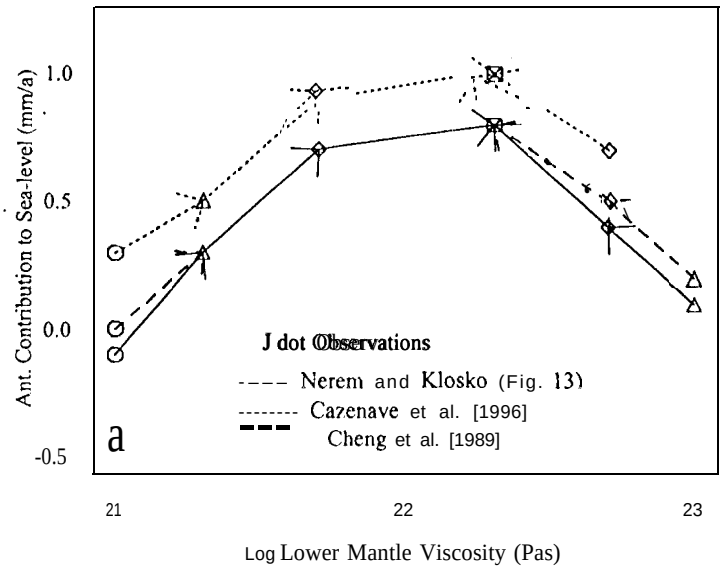
Ant. Contribution to Sea-level (mm/a)
1.0
0.5
0.0
-0.5
J dot Observations
---- Nerem and Klosko (Fig. 13)
------- Cazenave et al. [1996]
--- Cheng et al. [1989]
a
21
22
23
Log Lower Mantle Viscosity (Pas)

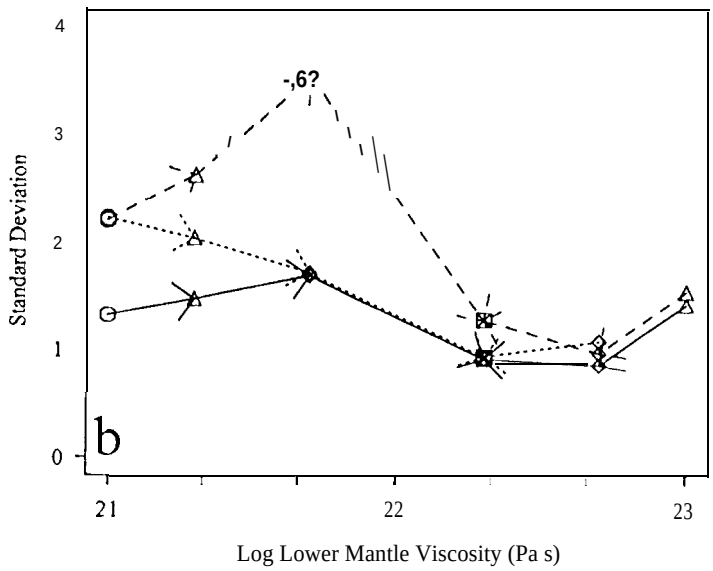
Standard Deviation
4
3
2
1
0
-,6?
b
21
22
23
Log Lower Mantle Viscosity (Pa s)

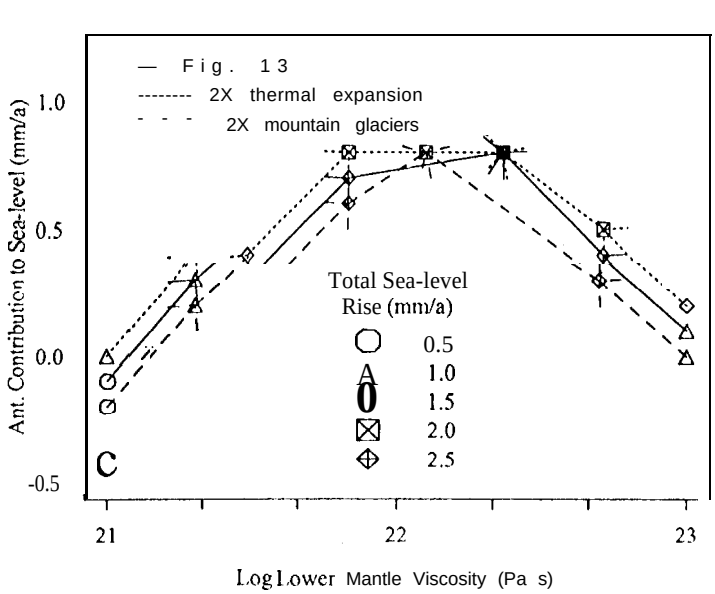
— Fig. 13
------- 2X thermal expansion
- - - 2X mountain glaciers
Ant. Contribution to Sea-level (mm/a)
1.0
0.5
0.0
-0.5
Total Sea-level Rise (mm/a)
0.5
1.0
1.5
2.0
2.5
c
21
22
23
Log Lower Mantle Viscosity (Pa s)

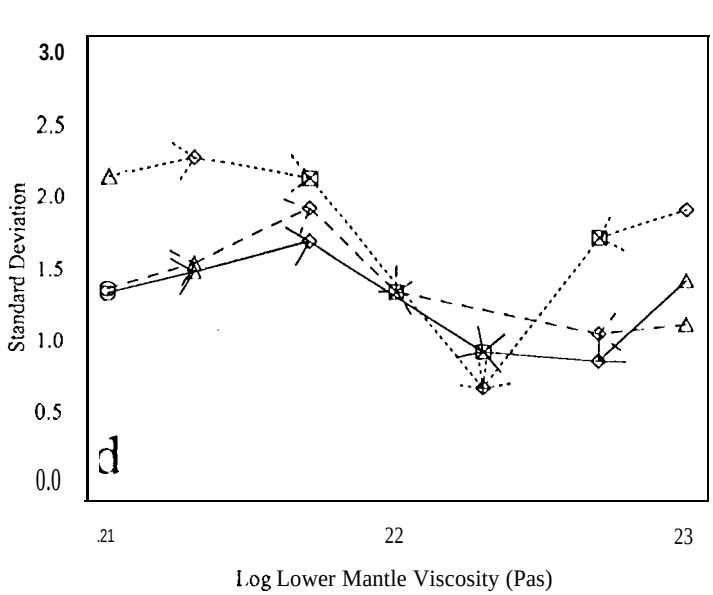
Standard Deviation
3.0
2.5
2.0
1.5
1.0
0.5
0.0
d
21
22
23
Log Lower Mantle Viscosity (Pas)

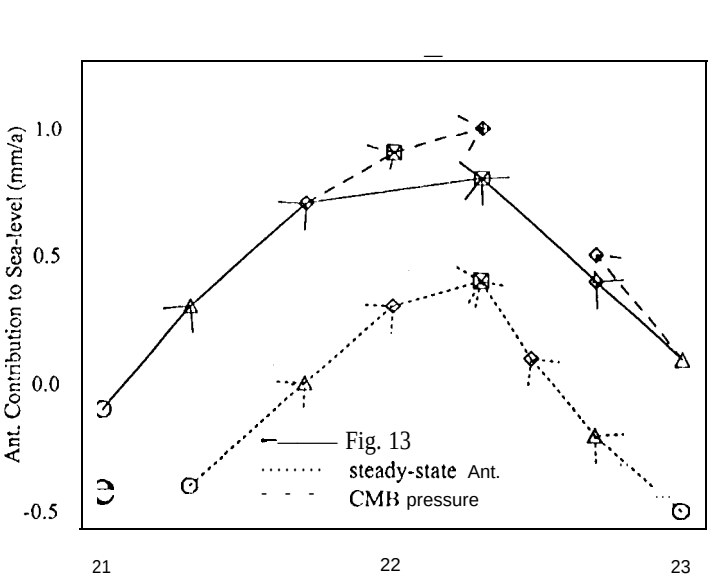
Ant. Contribution to Sea-level (mm/a)
1.0
0.5
0.0
-0.5
Fig. 13
steady-state Ant.
CMB pressure
e
21
22
23
Log Lower Mantle Viscosity (Pa s)

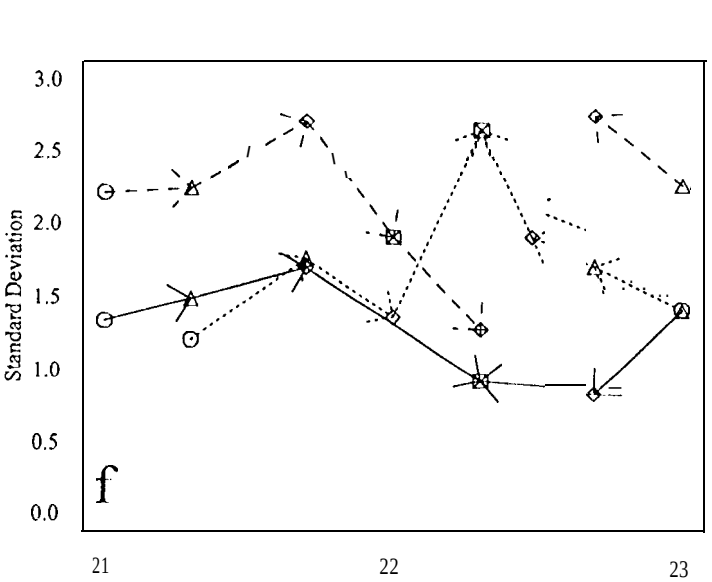
Standard Deviation
3.0
2.5
2.0
1.5
1.0
0.5
0.0
f
21
22
23
Log Lower Mantle Viscosity (Pa s)

Figure 15.

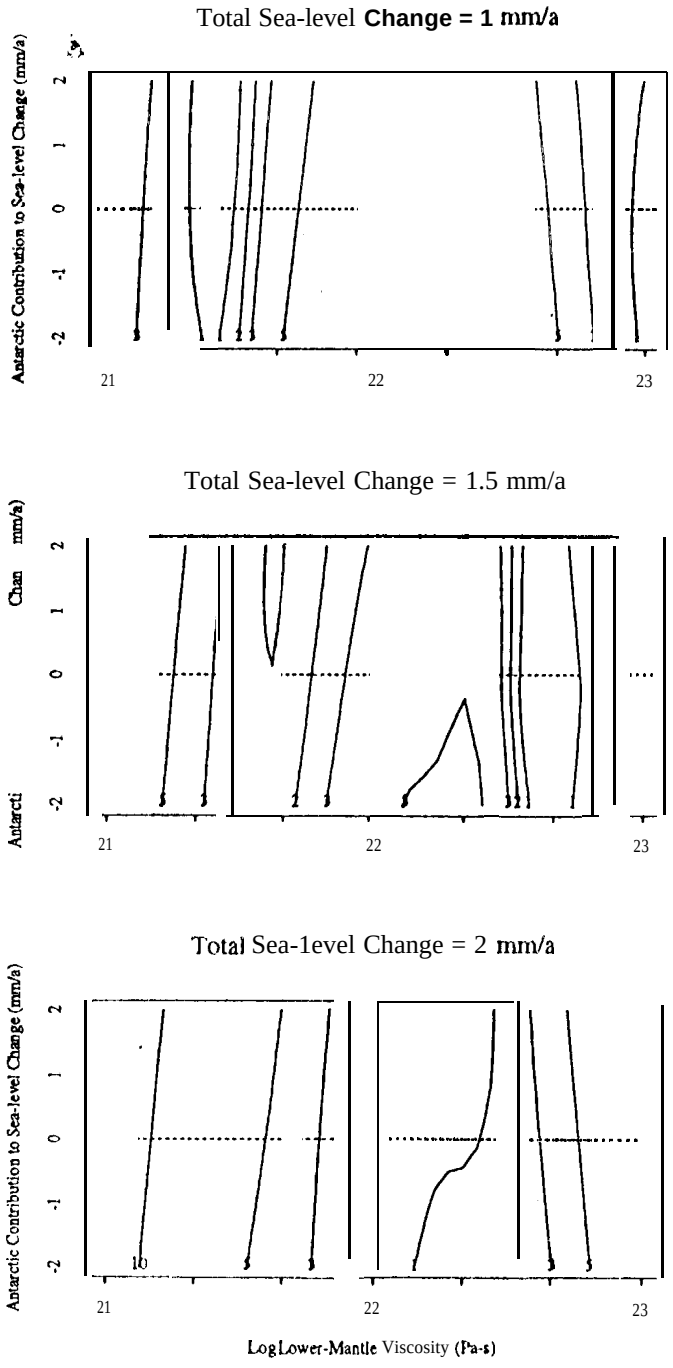
Total Sea-level Change = 1 mm/a
Antarctic Contribution to Sea-level Change (mm/a)
2
1
0
-1
-2
21
22
23
Total Sea-level Change = 1.5 mm/a
Chan mm/a)
Antarcti
Total Sea-1evel Change = 2 mm/a
Antarctic Contribution to Sea-level Change (mm/a)
Log Lower-Mantle Viscosity (Pa-s)

Figure 16.